



THE UNIVERSITY *of* EDINBURGH

Edinburgh Research Explorer

Behavioral-state modulation of inhibition is context-dependent and cell type specific in mouse visual cortex

Citation for published version:

Pakan, JMP, Lowe, SC, Dylida, E, Keemink, SW, Currie, SP, Coutts, CA & Rochefort, NL 2016, 'Behavioral-state modulation of inhibition is context-dependent and cell type specific in mouse visual cortex', *eLIFE*, vol. 5, e14985. <https://doi.org/10.7554/eLife.14985>

Digital Object Identifier (DOI):

[10.7554/eLife.14985](https://doi.org/10.7554/eLife.14985)

Link:

[Link to publication record in Edinburgh Research Explorer](#)

Document Version:

Peer reviewed version

Published In:

eLIFE

General rights

Copyright for the publications made accessible via the Edinburgh Research Explorer is retained by the author(s) and / or other copyright owners and it is a condition of accessing these publications that users recognise and abide by the legal requirements associated with these rights.

Take down policy

The University of Edinburgh has made every reasonable effort to ensure that Edinburgh Research Explorer content complies with UK legislation. If you believe that the public display of this file breaches copyright please contact openaccess@ed.ac.uk providing details, and we will remove access to the work immediately and investigate your claim.



1 **Behavioral-state modulation of inhibition**
2 **is context-dependent and cell type specific in mouse visual cortex**

3
4 Janelle M.P. Pakan¹, Scott C. Lowe², Evelyn Dylida¹, Sander W. Keemink^{2,3}, Stephen P. Currie¹,
5 Christopher A. Coutts¹, and Nathalie L. Rochefort¹

6
7 ¹Centre for Integrative Physiology, School of Biomedical Sciences, University of Edinburgh,
8 Edinburgh, EH8 9XD, United Kingdom.

9 ²Institute for Adaptive and Neural Computation, School of Informatics, University of
10 Edinburgh, Edinburgh, EH8 9AB, United Kingdom.

11 ³Bernstein Center Freiburg, Faculty of Biology, University of Freiburg, 79104 Freiburg,
12 Germany

13
14 Contact information:
15 Dr Nathalie Rochefort,
16 Centre for Integrative Physiology, Hugh Robson Building, University of Edinburgh,
17 Edinburgh, EH8 9XD, United Kingdom
18 n.rochefort@ed.ac.uk

19
20
21
22
23
24

25 **Abstract**

26 Cortical responses to sensory stimuli are modulated by behavioral state. In the primary
27 visual cortex (V1), visual responses of pyramidal neurons increase during locomotion. This
28 response gain was suggested to be mediated through inhibitory neurons, resulting in the
29 disinhibition of pyramidal neurons. Using *in vivo* two-photon calcium imaging in layers 2/3
30 and 4 in mouse V1, we reveal that locomotion increases the activity of vasoactive intestinal
31 peptide (VIP), somatostatin (SST) and parvalbumin (PV)-positive interneurons during visual
32 stimulation, challenging the disinhibition model. In darkness, while most VIP and PV neurons
33 remained locomotion responsive, SST and excitatory neurons were largely non-responsive.
34 Context-dependent locomotion responses were found in each cell type, with the highest
35 proportion among SST neurons. These findings establish that modulation of neuronal
36 activity by locomotion is context-dependent and contest the generality of a disinhibitory
37 circuit for gain control of sensory responses by behavioral state.

38

39 **Introduction**

40 Sensory perceptions are modulated by the context in which they are experienced. In
41 primary sensory areas, neuronal responses to sensory inputs are also modulated by
42 behavioral states, including level of arousal, attention and locomotion (Iriki et al., 1996;
43 Petersen and Crochet, 2013; Bennett et al., 2014; McGinley et al., 2015). *In vivo* recordings
44 in awake mice have shown that locomotion modulates the response properties of neurons
45 in the primary visual cortex (V1), resulting in an increased gain of excitatory neuron
46 responses to visual stimuli (Niell and Stryker, 2010; Keller et al., 2012; Bennett et al., 2013;
47 Polack et al., 2013; Saleem et al., 2013; Erisken et al., 2014; Reimer et al., 2014). However,
48 the neuronal circuits underlying this response modulation are unclear.

49 Recent studies have revealed that a specific subclass of inhibitory neurons,
50 expressing vasoactive intestinal peptide (VIP), strongly increase their activity during
51 locomotion (Fu et al., 2014; Reimer et al., 2014; Jackson et al., 2016). VIP neurons mainly
52 inhibit a second class of inhibitory neurons, expressing somatostatin (SST; Figure 1A; Pfeffer
53 et al., 2013; Jiang et al., 2015; Urban-Ciecko and Barth, 2016). It has been proposed that
54 cholinergic activation of VIP neurons during locomotion would inhibit SST neurons,
55 alleviating inhibition onto excitatory neurons and, as a consequence, increase the gain of
56 excitatory neuron visual responses (Figure 1B; Fu et al., 2014). However, a previous study
57 has reported an increase of SST spiking activity in layer 2/3 during locomotion (Polack et al.,
58 2013), an observation that challenges the hypothesis of an SST-cell mediated disinhibitory
59 circuit. The aforementioned recordings of SST neuronal activity were acquired in different
60 sensory contexts, either in darkness or during the presentation of visual stimuli. One
61 hypothesis that would explain the discrepancies between these results is that V1 neuronal
62 responses to locomotion are context-dependent.

63 In this study, we tested this hypothesis by directly comparing the locomotion
64 responses of excitatory and inhibitory neurons in darkness and during visual stimulation. We
65 used two-photon calcium imaging to monitor the activity of excitatory neurons as well as of
66 three non-overlapping populations of inhibitory neurons (VIP, SST and parvalbumin [PV]
67 neurons) in layer 2/3 and layer 4 of V1 in awake behaving mice. Our results show that during
68 visual stimulation these three classes of interneurons increase their activity with
69 locomotion, challenging the model of a disinhibitory circuit mediated through SST neurons.
70 We found that locomotion affects the activity of inhibitory circuits differently in darkness
71 and during visual stimulation, revealing a context-dependent, cell type specific response to
72 locomotion in V1. The highest proportion of context-dependent responses to locomotion

73 was found among SST neurons, which play a central role in V1 microcircuits. We suggest
74 alternative mechanisms of how locomotion modulates the neuronal activity in V1,
75 highlighting the dynamic nature of interneuron function that strongly depends on the
76 behavioral context of the animal.

77

78 **Results**

79 We compared the modulation of neuronal activity by locomotion in the mouse primary
80 visual cortex (V1), between two different sensory contexts: darkness and visual stimulation.
81 To do this, we used two-photon calcium imaging in head-fixed mice that ran freely on a
82 cylindrical treadmill (Figure 1C). The relative changes in somatic fluorescence of the
83 genetically-encoded calcium indicator GCaMP6f were used as a non-linear readout of the
84 neuronal spiking activity (Chen et al., 2013). Inhibitory neuronal subtypes were labeled by
85 injecting adeno-associated viruses (AAVs) into V1 of Cre-recombinase transgenic mice (PV-,
86 SST-, or VIP-Cre mice) for the Cre-inducible expression of the genetically-encoded
87 calcium indicator GCaMP6f (Figure 1D-E; Chen et al., 2013). To image excitatory neurons, we
88 co-injected a floxed version of GCaMP6f and an AAV where Cre expression is driven by a
89 CaMKII promoter, into C57/BL6 mice. After 2-3 weeks of expression, we recorded the
90 running speed and GCaMP6f signals simultaneously, both in total darkness and during visual
91 stimulation (Figure 1E).

92

93 Layer 2/3 cell type specific responses to locomotion differ in darkness and during visual
94 stimulation

95 *Excitatory neurons*

96 We quantified, for each excitatory neuron (n=1124 in 12 mice), the mean amplitude of
 97 calcium transients during locomotion periods and stationary periods, both during visual
 98 stimulation (drifting gratings) and in darkness (Figure 2A(i), B(i)). In agreement with previous
 99 electrophysiological observations (Niell and Stryker, 2010; Keller et al., 2012; Bennett et al.,
 100 2013; Polack et al., 2013; Saleem et al., 2013; Erisken et al., 2014; Reimer et al., 2014), we
 101 observed that, on average, locomotion increased the amplitude of calcium transients in
 102 excitatory neurons during visual stimulation (Figure 2B(i), Figure 2-figure supplement 1B(i)
 103 mean change in fluorescence $[\Delta F/F_0] = 0.12 \pm 0.02$ locomotion versus 0.07 ± 0.01 stationary;
 104 $p < 0.001$, n=12, Wilcoxon signed rank test). We quantified the effect of locomotion by
 105 calculating a locomotion modulation index (LMI) for each neuron, corresponding to the
 106 difference between the mean $\Delta F/F_0$ during locomotion (R_L) and stationary (R_s) periods,
 107 normalized by the sum of the mean $\Delta F/F_0$ during both behavioral states ($LMI = (R_L - R_s)/(R_L +$
 108 $R_s)$). An LMI equal to 0 indicates no difference between locomotion and stationary periods,
 109 while an LMI equal to 0.5 indicates that the average amplitude of calcium transients was
 110 three times higher during locomotion than during stationary periods. Comparing the
 111 distribution of LMIs between the two sensory contexts, we found that the modulation of
 112 activity of excitatory neurons by locomotion was significantly different in darkness
 113 compared to visual stimulation (Figure 2C(i), D(i); mean of median LMI: 0.07 ± 0.02 darkness
 114 versus 0.19 ± 0.02 visual stimulation; $p = 0.001$, n=12, Kruskal–Wallis test). During visual
 115 stimulation, $47 \pm 4\%$ of excitatory neurons were significantly locomotion responsive (see
 116 Material and methods for locomotion responsive criteria), compared with $28 \pm 4\%$ in
 117 darkness. Additionally, in the dark, a small proportion of neurons were inhibited by
 118 locomotion, decreasing their activity during locomotion periods relative to stationary
 119 periods ($10 \pm 1\%$ of neurons).

VIP neurons

As reported in previous studies (Fu et al., 2014; Reimer et al., 2014; Jackson et al., 2016), we found that VIP neurons (n=210 in 12 mice) strongly responded to locomotion (Figure 1E and Figure 2A(ii), B(ii)). This was true both in darkness (mean $\Delta F/F_0 = 0.51 \pm 0.12$ locomotion versus 0.10 ± 0.03 stationary; $p < 0.001$, n=12, Wilcoxon signed rank test) as well as during visual stimulation (mean $\Delta F/F_0 = 0.42 \pm 0.14$ locomotion versus 0.09 ± 0.02 stationary; $p < 0.001$, n=12) with no significant difference in the average LMI between sensory contexts (Figure 2C(ii), D(ii), mean of median LMI: 0.60 ± 0.05 darkness versus 0.49 ± 0.06 visual stimulation; $p = 0.106$, n=12, Kruskal–Wallis test; see also Figure 2-figure supplement 1B(ii)). A high proportion of VIP neurons were significantly locomotion responsive in both sensory contexts ($85 \pm 7\%$ in darkness and $79 \pm 6\%$ during visual stimulation).

In order to compare our results directly with previous findings (Fu et al., 2014), we calculated the cross-correlation between VIP calcium signals and running speed. We confirmed the presence of a single positive peak around time zero, both in darkness and during visual stimulation (Figure 2-figure Supplement 3A(ii), B(ii)). We also observed a lower amplitude during visual stimulation but this decrease was not significant (mean zero-time correlation: 0.26 ± 0.04 in darkness versus 0.20 ± 0.02 during visual stimulation; $p = 0.225$, n=12, Kruskal–Wallis test; Figure 2-figure Supplement 3C). Similarly, the mean $\Delta F/F_0$ (Figure 2-figure supplement 2C(ii)) and the mean LMI (Figure 2D(ii)) of VIP neurons also decreased during visual stimulation, without reaching significance (mean $\Delta F/F_0 = 0.51 \pm 0.12$ in darkness versus 0.42 ± 0.14 during visual stimulation; $p = 0.151$, n=12, Wilcoxon signed rank test).

SST neurons

In contrast to VIP neurons, responses of SST neurons (n=79 in 11 mice) to locomotion were found to be highly context-dependent. During visual stimulation, the mean $\Delta F/F_0$ during locomotion periods was significantly higher than during stationary periods (Figure 2B(iii), Figure 2-figure supplement 1B(iii); mean $\Delta F/F_0 = 0.25 \pm 0.05$ locomotion versus 0.10 ± 0.03 stationary; $p=0.001$, $n=11$, Wilcoxon signed rank test). However, in darkness, SST neurons were either non-responsive, increased or even decreased their activity during locomotion with, on average, no significant difference between locomotion and stationary periods (Figure 2A(iii), Figure 2-figure supplement 1B(iii); mean $\Delta F/F_0 = 0.06 \pm 0.02$ locomotion versus 0.06 ± 0.01 stationary; $p=0.102$, $n=11$, Wilcoxon signed rank test). As a result, the modulation of SST neuron responses by locomotion was found to be significantly different across sensory contexts (Figure 2C(iii), D(iii), mean of median LMI: 0.06 ± 0.04 darkness versus 0.33 ± 0.06 visual stimulation; $p=0.002$, $n=11$, Kruskal–Wallis test). During visual stimulation, $63 \pm 7\%$ of SST neurons were significantly locomotion responsive (increasing their activity) and only $4 \pm 3\%$ were decreasing their activity during locomotion. In darkness, the percentage of neurons increasing their activity dropped to $24 \pm 6\%$ with an additional $11 \pm 5\%$ of SST neurons decreasing their activity during locomotion.

In line with these results, the cross-correlation between SST calcium transients and running speed significantly increased during visual stimulation compared to darkness (mean zero-time correlation = 0.04 ± 0.01 in darkness versus 0.13 ± 0.01 during visual stimulation; $p=0.001$, $n=11$, Kruskal–Wallis test; Figure 2-figure supplement 3C). Notably, SST neurons were strongly responsive to visual stimulation (Figure 2-figure supplement 2(iii); mean $\Delta F/F_0$ during locomotion = 0.06 ± 0.02 darkness versus 0.25 ± 0.05 visual stimulation; $p=0.001$, $n=11$, Wilcoxon signed rank test). These results indicate that most SST neurons respond to visual stimuli and, in addition to this visual response, they become responsive to

locomotion. In darkness, however, they have low spontaneous activity and are largely non-responsive to locomotion (Figure 2E).

PV neurons

Finally, PV neurons (n=199 in 13 mice) were strongly responsive to locomotion in both sensory contexts (Figure 2A(iv), B(iv), Figure 2-figure supplement 1B(iv); dark: mean $\Delta F/F_0 = 0.33 \pm 0.07$ locomotion versus 0.13 ± 0.02 stationary; $p=0.001$; visual stimulation: mean $\Delta F/F_0 = 0.41 \pm 0.08$ locomotion versus 0.16 ± 0.03 stationary; $p<0.0001$; n=13 Wilcoxon signed rank test), with no significant difference between sensory conditions (Figure 1E, Figure 2C(iv), D(iv); mean of median LMI: 0.32 ± 0.06 darkness versus 0.35 ± 0.04 visual stimulation; $p=0.663$, n=13, Kruskal–Wallis test). Similarly, the cross-correlation between running speed and calcium transients showed a positive peak around time zero both in darkness and during visual stimulation, with no significant difference ($p=0.778$; n=13, Kruskal–Wallis test; Figure 2-figure supplement 3).

Modulation of neuronal responses by locomotion during patterned and non-patterned visual stimuli

Isoluminant grey screen stimulation is commonly used to record so called ‘spontaneous activity’ of neurons in the visual cortex. Since our results showed different locomotion responses in the dark and during the presentation of drifting gratings, we tested whether this difference was due to the presence of patterned visual stimuli or, more simply, to the presence of light (Figure 2-figure supplement 1). We quantified the amplitude of fluorescence changes during stationary and locomotion periods in all three contexts: darkness, grey screen and drifting gratings. We did not find any significant difference for any

of the inhibitory populations (VIP, SST and PV neurons) between the two types of visual stimulation (gratings vs grey screen; Figure 2-figure supplement 1C). For excitatory neurons, we found a lower LMI during the presentation of a grey screen than during drifting grating presentation (mean of median LMI: 0.17 ± 0.02 grey versus 0.19 ± 0.02 visual stimulation; $p=0.033$, $n=12$, Kruskal–Wallis test; Figure 2-figure supplement 1C(i)). Locomotion responses for each type of visual stimulus (gratings vs grey screen) were still significantly higher than during darkness (mean of median LMI: 0.07 ± 0.02 dark versus 0.17 ± 0.02 grey; $p=0.007$, $n=12$, Kruskal–Wallis test) (Figure 2-figure supplement 1C(i)). These results indicate that, during visual stimulation and independently of the presence of patterned visual stimuli, excitatory, VIP, SST and PV neurons show increased activity during locomotion.

Diversity of context-dependent locomotion responses within cell types

While comparisons of a neuronal population's LMI distribution (Figure 2C) indicates how, on average, that cell type is modulated by locomotion in different sensory contexts, it does not provide information about the context-dependent responses of single neurons. For instance, the average LMI could be the same in darkness and during visual stimulation even though individual neurons may have large changes in their LMI, which cancel out when considering the population as a whole.

In order to show the diversity of locomotion responses within each neuronal subtype, we examined the LMI value in darkness versus during visual stimulation for each neuron (Figure 3A). Neurons near the identity line show context-independent locomotion responses (similar LMI in darkness and during visual stimulation), while the other neurons changed their response to locomotion from one context to another (context-dependent responses). We first quantified this diversity by calculating the difference between the LMI

value during visual stimulation and the LMI value in darkness for each neuron (Figure 3B). These results confirmed that VIP neurons displayed mainly context-independent locomotion responses (Figure 3B(ii), narrow distribution, centered around 0), while locomotion responses of SST neurons were mainly context dependent (Figure 3B(iii), broad distribution shifted towards positive values). Both excitatory and PV neuronal populations included a diversity of locomotion responses (broad distributions). To quantify the proportions of context-independent and context-dependent neurons in each cell type, we first determined the variability of the locomotion responses for each context by comparing neuronal responses across odd and even locomotion periods (Figure 3-figure supplement 1; see Materials and methods). We found high correlation values for all neuronal populations, both in darkness and during visual stimulation ($0.676 < R < 0.944$; $p < 0.0001$), indicating a general low variability of the responses across different locomotion periods in both contexts. We determined the proportion of context-dependent neurons meeting two criteria: i) with a response that was significantly different across contexts (neurons distance from the identity line in Figure 3A, to estimate the error on the LMI in both dark and stimulated conditions for each neuron, bootstrapping was employed (see Materials and methods)), and ii) with low variability of locomotion responses (Figure 3-figure supplement 1).

These results confirm that most VIP neurons were context-independent, remaining locomotion-responsive in both sensory contexts (66%), with only 17% of neurons showing context-dependent responses (Figure 3A(ii), Figure 3-figure supplement 2). The proportion of context-dependent neurons was the highest among SST neurons, with 49% of neurons showing context-dependent responses to locomotion (Figure 3A(iii), Figure 3-figure supplement 2). Both excitatory and PV neurons had approximately the same proportion of context-dependent neurons (22% for excitatory and 25% for PV neurons) (Figure 3A(i), (iv)).

240 Finally, we tested whether context-dependent neurons differ from context-
241 independent ones with regard to the following characteristics: percentage of visually
242 responsive neurons, orientation selectivity and direction selectivity. We did not find any
243 significant difference in any neuronal population (comparisons between context-dependent
244 and context independent neurons for each cell type, OSI, $p>0.261$; DSI $p>0.093$, Kruskal–
245 Wallis test), suggesting that the mechanisms underlying the modulation of locomotion
246 responses differ from those determining the selectivity of visual responses.

247

248 Layer 4 excitatory and inhibitory responses to locomotion are similar to layer 2/3

249 Layer 2/3 neurons receive sensory information from excitatory neurons in layer 4, the main
250 thalamo-recipient layer, as well as top-down information from higher cortical areas (Niell,
251 2015). In addition, these neurons receive subcortical inputs from the dorsal lateral
252 geniculate nucleus as well as neuromodulatory inputs (Polack et al., 2013; Fu et al., 2014;
253 Lee et al., 2014). Context-dependent locomotion responses of layer 2/3 neurons may thus
254 come from one of these distinct inputs or from a combination of them. By using the same
255 approach as for layer 2/3 neurons, we recorded locomotion responses in layer 4 neurons
256 (excitatory $n=331$; VIP $n=57$; SST $n=74$; PV $n=109$; in 6, 4, 6 and 6 mice, respectively). As in
257 layer 2/3, we used local injections of AAVs into V1 for the Cre-inducible expression of the
258 genetically-encoded calcium indicator GCaMP6f. However, we observed that on average the
259 GCaMP6f labelling in layer 4 was sparser than in layer 2/3 (Figure 1D). Thus, we cannot
260 exclude that we preferentially labelled subtypes of layer 4 neurons in which transduction
261 efficiency with these AAV vectors would be higher. The quantification of locomotion
262 responses showed no significant difference between layer 2/3 and layer 4 neurons, in any
263 cell type, both in darkness and during visual stimulation (Figure 4B, C). The results showed a

higher mean LMI value for PV neurons in layer 4 (0.45 ± 0.04) compared to layer 2/3 (0.35 ± 0.04) during visual stimulation. However, this did not reach significance; $p=0.058$, Mann-Whitney U-test). In addition, the results showed similar proportions of context-dependent responses in layer 4 as described in layer 2/3 (Figure 4A, see also Figure 3A; context-dependent neurons: Exc, L2/3: 22%, L4: 17%; VIP, L2/3: 17%, L4: 26%; SST, L2/3: 49%, L4: 42%; PV, L2/3: 25%, L4: 23%).

Discussion

The increased gain of visual responses during locomotion provides a model to elucidate the circuit mechanisms underlying behavioral-state dependent changes of sensory responses. In this study, we found that the modulation of neuronal activity by locomotion is context-dependent and cell type specific, in layer 2/3 and layer 4 of mouse V1. During periods of visual stimulation, locomotion increases the activity of excitatory neurons as well as of three classes of inhibitory neurons (VIP, SST, PV; Figure 2E). These results indicate that the enhancement of excitatory neuron visual responses during locomotion does not result from the inhibition of SST neurons, in mouse V1. Our findings thus challenge the generality of a disinhibitory circuit involving VIP, SST and pyramidal neurons for the gain control of sensory responses by behavioral state.

Relationship between somatic fluorescence changes and spiking activity in different neuronal types and behavioral contexts

In this study, we used the relative changes in fluorescence of the genetically-encoded calcium indicator GCaMP6f as a reporter of the spiking activity of cortical neurons (Chen et al., 2013). For a given fluorescent calcium indicator, the relationship between the amplitude

of somatic fluorescence changes and the number of spikes can be affected by a number of factors including the concentration of calcium buffers in the soma, the balance between calcium influx and efflux as well as calcium release from internal stores (Grienberger et al., 2012). Consequently, potential confounding factors in the present study would be (1) different intracellular calcium dynamics in different types of inhibitory neurons as well as (2) a higher increase of cytosolic free calcium concentration for the same number of spikes during locomotion compared to stationary periods. Considering that neuromodulators can regulate calcium influx (Fucile, 2004; Shen and Yakel, 2009), this second possibility may result from the action of neuromodulators released during locomotion that would increase the amount of calcium entering the neuron in response to each spike. In that case, for the same number of spikes, the increase in fluorescence of our calcium indicator would be higher during locomotion than during stationary periods.

Without an independent readout of the spiking activity for each neuronal type in each behavioral context, we cannot exclude that the relationship between fluorescence transients and number of spikes differ between different neurons and different contexts. However, the comparison of our results (mean $\Delta F/F_0$, Figure 2-figure supplement 1B, 'stim' column) with spiking frequencies published in a previous study (see Supplementary Table 3 of Polack et al., 2013) in mouse V1 strongly suggests that somatic GCaMP6f fluorescence changes do reflect changes in spiking activity related to locomotion. For the same neuronal populations (layer 2/3 Excitatory, SST and PV neurons; layer 4 Excitatory neurons) and visual stimulation condition (drifting gratings), both data sets show the same relative change in signal during locomotion compared to stationary periods (corresponding to an approximate doubling of activity during locomotion for all three cell types). This similarity suggests that

somatic GCaMP6 fluorescence changes during locomotion do reflect changes in spiking activity, at least in these cell types during visual stimulation.

Comparison with previous findings: locomotion responses differ in darkness and during visual stimulation

In this study, we found that SST activity increased with locomotion during visual stimulation. This is in line with previous electrophysiological recordings of SST neurons (Polack et al., 2013) but in contradiction with the current disinhibitory model that relies on the inhibition of SST neurons during locomotion (Figure 1B; Fu et al., 2014). Our results provide an explanation for these discrepancies since the aforementioned electrophysiological recordings were acquired during visual stimulation whereas imaging of SST activity was done in the dark (Fu et al., 2014). The disinhibitory model was based on the assumption that the locomotion-driven response of SST neurons would be similar in the dark and during visual stimulation (Fu et al., 2014). The same assumption was made in the interpretation of membrane potential fluctuations of VIP and SST neurons recorded during the presentation of a blank screen (Reimer et al., 2014). While VIP neurons were reliably depolarized during running, the SST population was heterogeneous. The authors distinguished two populations of SST interneurons (see Supplementary Figure 5C of Reimer et al., 2014): Type I cells were inhibited by running while Type II cells were depolarized. Importantly, spiking activity of SST neurons was not reported and it is thus not clear how the membrane potential fluctuations relate to spiking activity.

Our findings regarding the locomotion responses of SST neurons in darkness are consistent with the previous imaging study performed in similar conditions (Figure 2-figure supplement 3 of the present study compared to Figure 3 and Figure S3 of Fu et al., 2014) as

well as with the heterogeneity of membrane potential fluctuations of SST neurons during locomotion (Reimer et al., 2014). We cannot exclude the possibility that a disinhibitory circuit may underlie the activity of a small fraction of neurons in darkness: the majority of VIP neurons increase their activity with locomotion, while a small proportion of SST neurons are inhibited during locomotion, potentially leading to the increase in activity of some pyramidal neurons. However, the results obtained in darkness show that the majority of SST neurons are not responsive to locomotion at all, challenging the generality of a disinhibitory circuit acting through the inhibition of SST neurons. With visual stimulation, the inconsistency of the disinhibitory model is even stronger since the vast majority of SST neurons increase their activity with locomotion (see Figure 2B(iii)). Consequently, the results obtained during visual stimulation (present study and Polack et al., 2013) are incompatible with a model in which VIP neurons disinhibit excitatory neurons by inhibiting SST neurons. Additionally, while the vast majority of VIP neurons are context-independent with regard to their locomotion response, excitatory neurons show significantly increased locomotion responses during visual stimulation compared to darkness conditions. Therefore, the context-dependent responses of excitatory neurons do not result from a disinhibitory circuit initiated by VIP neurons.

An appealing aspect of the disinhibitory model was the idea of a canonical circuit for gain modulation of sensory responses (Pi et al., 2013). While the connectivity may be canonical, we show that the circuit activity can strongly differ depending on the behavioral context. Therefore, functional properties of inhibitory neurons should not be generalized from one context to the next, and caution should be taken when inferring connectivity from functional recordings obtained in a specific behavioral context.

Alternative circuit mechanisms for behavioral-state modulation of visual responses in V1

Our results indicate that, in addition to the activation of VIP neurons during locomotion, other pathways are involved in linking locomotion and visual responses in V1. We suggest that neuromodulatory inputs triggered by locomotion would not only activate VIP neurons through nicotinic acetylcholine receptors as previously shown (Alitto and Dan, 2013; Arroyo et al., 2014; Fu et al., 2014), but would also directly activate PV, SST, and excitatory neurons. Previous work has demonstrated cholinergic facilitation of cortical inhibitory neurons (Kawaguchi, 1997; Xiang et al., 1998; Arroyo et al., 2012; Alitto and Dan, 2013), including SST neurons (Kawaguchi, 1997; Fanselow et al., 2008; Xu et al., 2013; Chen N. et al., 2015). Similarly, *in vitro* studies have shown that norepinephrine can depolarize both excitatory (McCormick et al., 1993; Kirkwood et al., 1999) and inhibitory (Kawaguchi and Shindou, 1998) cortical neurons. Finally, *in vivo* studies have shown that neuromodulatory inputs, cholinergic and noradrenergic, can control the gain and signal-to-noise ratio of V1 excitatory neurons during locomotion (Pinto et al., 2013; Polack et al., 2013; Bennett et al., 2014; Lee et al., 2014). We suggest that in darkness, the effect of neuromodulatory inputs remains subthreshold in SST neurons. During visual stimulation, SST neurons are strongly activated and the effect of neuromodulatory inputs becomes suprathreshold. In agreement with the known intra-cortical connectivity in mouse V1 (Figure 1A; Pfeffer et al., 2013; Jiang et al., 2015), our findings support this neuromodulatory hypothesis. In darkness, VIP and PV neurons are activated by locomotion and inhibit SST and excitatory neurons, preventing their activation by locomotion-dependent inputs. During visual stimulation, SST and excitatory neurons are activated: they overcome the intra-cortical inhibition by VIP and PV neurons and become responsive to direct locomotion-dependent inputs. Since SST neurons provide the main intra-cortical input to VIP neurons (Pfeffer et al., 2013) and are strongly

visually-responsive, they likely inhibit VIP neurons (or a subpopulation of VIP neurons) during visual stimulation. This is consistent with the decrease in activity of a portion of VIP neurons that was observed during visual stimulation (Fu et al., 2014; see also Figure 2-figure supplement 2B(ii)).

An alternative or complementary hypothesis to the neuromodulatory pathway is that the modulation of visual inputs by locomotion already takes place in subcortical nuclei, such that the thalamo-cortical inputs received by excitatory neurons, and potentially SST neurons, would convey the increased gain of visual responses during locomotion. Indeed, recent studies have shown that projections from the dorsal lateral geniculate nucleus (Erisken et al., 2014; Roth et al., 2016) and from the thalamic latero-posterior nucleus (Roth et al., 2016) to V1 both convey locomotion signals.

The diversity of context-dependent responses to locomotion within SST, PV and, to a lesser extent, VIP populations indicates that there are functional sub-types within each of these interneuron populations. Based on a comprehensive analysis of morphological and electrophysiological properties of inhibitory neurons, a recent *in vitro* study has identified seven distinct types of cortical interneurons in layer 2/3 (Jiang et al., 2015). Further *in vivo* characterization of the activity of these sub-types will be necessary to identify how these populations relate to the different context-dependent responses identified in the present study.

Materials and methods

Animals

Three Cre-driver transgenic mice lines were used to label inhibitory interneurons: *Sst*<tm2.1(cre)Zjh> (SST-Cre) [RRID:IMSR_JAX:013044], *Pvalb*<tm1(cre)Arbr> (PV-Cre)

[RRID:IMSR_JAX:008069], *Vip*^{tm1(cre)Zjh} (VIP-Cre) [RRID:IMSR_JAX:010908], all originally obtained from Jackson Laboratory, ME, USA. These lines were cross-bred with Rosa-CAG-LSL-tdTomato [RRID:IMSR_JAX:007914] mice. C57Bl/6 wild type mice (Jackson Laboratory, ME, USA) were used for virus injections targeting the expression of GCaMP6 in CaMKII-expressing neurons. Mice were group housed (typically 2–4 mice) and both male and female mice were used for the experiments. All procedures were approved by the University of Edinburgh animal welfare committee, and were performed under a UK Home Office project license.

Surgical procedures

Virus injections

For virus injections, 8- to 10-week-old mice were anaesthetized with isoflurane (4% for induction and 1-2% maintenance during surgery) and mounted on a stereotaxic frame (David Kopf Instruments, CA, USA). Eye cream was applied to protect the eyes (Bepanthen, Bayer, Germany) and analgesics were injected subcutaneously (Vetergesic, buprenorphine, 0.1 mg/kg of body weight). After an incision was made in the scalp, the bone surface was cleaned and a small craniotomy was performed over the left V1 (3.5 mm lateral and 1 mm anterior to lambda with an injection pipette inserted 70° from vertical and 30° from midline). Adeno-associated viruses (AAVs) were injected using a pipette with 20 µm tip diameter (Nanoject, Drummond Scientific, PA, USA) at a speed of 10 nl min⁻¹ at three different depths (around 250, 400, and 600 µm deep; 50 nl per site). AAVs used in this study include: AAV1.Syn.Flex.GCaMP6f.WPRE.SV40 to label SST, PV, and VIP cells in Cre-driver transgenic mice as well as AAV1.Syn.GCaMP6f.WPRE.SV40 in tdTomato crosses (see above) and AAV1.CaMKII0.4.Cre.SV40 with AAV1.Syn.Flex.GCaMP6f.WPRE.SV40 in C57Bl/6 wild

type mice (all AAVs acquired from the University of Pennsylvania Vector Core, PA, USA). After each injection, pipettes were left in situ for an additional 5 min to prevent backflow. The skin was then sutured and mice were monitored until they recovered from anesthesia. Animals were returned to their home cage for 2-3 weeks.

Head-plate and imaging window

Mice were anesthetized with isoflurane (4% for induction and 1-2% maintenance during surgery) and mounted in a stereotaxic frame. Eye cream was applied to protect the eyes (Bepanthen, Bayer, Germany), analgesics and anti-inflammatory drugs were injected subcutaneously (Vetergesic, buprenorphine, 0.1 mg/kg of body weight, carprofen, 0.15mg, and dexamethasone, 2µg). A section of scalp was removed and the underlying bone was cleaned before a craniotomy (around 2x2 mm) was made over the left V1 (centred around 2.5 mm lateral and 0.5 mm anterior to lambda). The craniotomy was then sealed with a glass cover slip and fixed with cyano-acrylic glue. A custom-built head-post was implanted on the exposed skull with glue and cemented with dental acrylic (Paladur, Heraeus Kulzer, Germany).

Two-photon calcium imaging

Imaging was performed using a custom-built resonant scanning two-photon microscope with a Ti:Sapphire pulsing laser (Chameleon Vision-S, Coherent, CA, USA; < 70 fs pulse width, 80 MHz repetition rate) tuned to 920 nm. Using a 40X objective (0.8 NA, Nikon), 600x600 pixel images with a field-of-view of 250x250 µm were acquired at 40 Hz with custom-programmed LabVIEW based software (version 8.2; National Instruments, UK).

454 We used two-photon calcium imaging in head-fixed mice that ran freely on a
455 cylindrical treadmill (Figure 1C; Dombek et al., 2007). Habituation and imaging started 2-3
456 weeks after AAV injection. Mice were habituated to head-fixation in the dark for 45 min and
457 began to run freely on a polystyrene cylinder (20 cm diameter, on a ball-bearing mounted
458 axis). The mice's running speed on the circular treadmill was continuously monitored using
459 an optical encoder (E7P, 250cpr, Pewatron, Switzerland) connected to a data acquisition
460 device (National Instrument, UK) with custom-written software in LabView (National
461 Instrument, UK) and analyzed in MATLAB (Mathworks, MA, USA). Mice could run freely and
462 spent on average $26 \pm 2\%$ of the time running in the dark and $41 \pm 2\%$ during visual
463 stimulation ($n = 48$ mice, 51 sessions).

464 Two-photon imaging was performed at 2-3 focal planes per mouse, at cortical depths
465 between 130–350 μm for L2/3 neurons and 350–500 μm for L4 neurons (cortical layers
466 were confirmed on histological sections, see below). Laser power at the brain surface was
467 kept below 50 mW. Mice with excessive brain movement artefacts were excluded. At each
468 focal plane ($n = 100$ fields of view), 8-12 trials (60 s duration) were acquired in total darkness
469 and 12-20 trials acquired during visual stimulation, with dark and visual stimulation trials
470 randomly interleaved.

471 Visual stimuli were generated using the Psychophysics Toolbox package (Brainard,
472 1997) for MATLAB (Mathworks, MA, USA) and displayed on an LCD monitor (51×29 cm, Dell,
473 UK) placed 20 cm from the right eye, covering $104^\circ \times 72^\circ$ of the visual field. Visual stimulation
474 trials consisted of stationary full-field square-wave gratings for 4-5 s and the corresponding
475 drifting phase for 2 s (0.03 cpd, 1 Hz, 8 equally spaced directions in randomized order,
476 contrast 80%, mean luminance 37 cd/m^2). Each trial started and ended with a grey screen
477 (isoluminance). Additional grey screen data presented in Figure 2-figure supplement 1 were

obtained during the presentation of an isoluminant grey screen for 5-15 s. preceding the presentation of each oriented grating for 5 s (0.03 cpd, 1 Hz, 4 equally spaced orientations in randomized order, contrast 80%, mean luminance 37 cd/m²).

At the end of the imaging session, red retrograde beads (Lumafluor, USA) were injected either at the surface or at 2 different focal planes at which neurons had been imaged. This red labelling was used as a structural landmark in histological sections to confirm which cortical layers had been imaged.

Histology

Animals were transcardially perfused with 0.9% saline and 4% PFA in phosphate buffer (0.1M). Brains were sliced with a vibratome (50 µm thick) and rinsed in phosphate buffered saline (PBS). The slices were then mounted and counterstained with either DAPI (Vectashield mounting medium, Vector Labs, UK) or NeuroTrace 640/660 fluorescent Nissl stain (1:2000; RRID:nlx_152414, Life Technologies, NY, USA) and coverslipped. Sections were imaged with a confocal microscope (Nikon A1R, Nikon Instruments, UK) to define the boundaries of cortical layers and localize the retrograde beads injected at the imaged focal planes *in vivo*.

Data analysis

Image Analysis

To correct for brain motion after image acquisition, we used 2D plane translation-based image alignment (SIMA 1.2.0, sequential image analysis; Kaifosh et al., 2014). Regions of interest (ROIs) corresponding to neuronal cell bodies were selected manually by inspecting down-sampled frames (2 Hz), as well as the maximum intensity projection of each imaging

stack (60 s trial). Pixel intensity within each ROI was averaged to create a raw fluorescence time series $F(t)$. Baseline fluorescence F_0 was computed for each neuron by taking the 5th percentile of the smoothed $F(t)$ (1Hz lowpass, zero-phase, 60th-order FIR filter) over each trial ($F_0(t)$), averaged across all trials. As a consequence, the same baseline F_0 was used for computing the changes in fluorescence in darkness and during visual stimulation. The change in fluorescence relative to baseline, $\Delta F/F_0$ was computed by taking the difference between F and $F_0(t)$ and dividing by F_0 . In order to remove neuropil contamination, we used nonnegative matrix factorization (NMF), which is a low rank matrix decomposition method used for demixing spatially overlapping signal sources (Kim and Park, 2007; Langville et al., 2014), as implemented in NIMFA 1.2.1 (Žitník and Zupan, 2012). The Python toolboxes were run with WinPython 2.7.10.3. All further analyses were performed using custom-written scripts in MATLAB (MathWorks, MA, USA).

Analysis of Locomotion Responses

Changes in the position of the cylindrical treadmill (sampled at 12,000 Hz) were interpolated onto a downsampled rate of 40 Hz, matching the sampling rate of the two-photon imaging. To define stationary and locomotion periods we used the following criteria. Stationary corresponded to periods where instantaneous speed (as measured at the 40 Hz sampling rate) was less than 0.1 cm/s. Locomotion corresponded to periods meeting three criteria: instantaneous speed ≥ 0.1 cm/s, 0.25Hz lowpass filtered speed ≥ 0.1 cm/s, and an average speed ≥ 0.1 cm/s over a 2 second window centered at this point in time. Any inter-locomotion interval shorter than 500 ms was also labelled as locomotion. Stationary periods less than 3 s after or 0.2 s before a period of locomotion were removed from the analysis. The locomotion modulation index (LMI) was defined as the difference between the mean

$\Delta F/F_0$ during locomotion (R_L) and stationary (R_S) periods, normalized by the sum of both values: $LMI = (R_L - R_S)/(R_L + R_S)$.

To estimate the error on the LMI in both dark and stimulated conditions for each neuron, bootstrapping with sample replacement was employed. We binned the signal into 1 s bins, each of which had only one visual stimulus and one behavioral activity (locomotion or stationary) throughout its duration. For each 1 s bin, we took the mean $\Delta F/F_0$ and regarded this value as a single sample. For periods of time which had a single stimulus and behavioral activity persisted for longer than 1 s, additional samples were drawn with intervals of no less than 2 s. This interval duration was selected based on the autocorrelation of the calcium fluorescence signal, which took approximately 2 s to fall to 0.5. The average correlation between consecutive samples of the same stimulus and activity condition was computed as a weighted average over all conditions, and was found to be $R = 0.35$. We then randomly selected samples of $\Delta F/F_0$ with replacement from our original set of samples. The number of samples selected in each bootstrap resample ($65\% = 1-R$) was reduced from the total number of samples available to reflect the fact that our samples were not completely independent. This process was repeated 10000 times to obtain 95% confidence intervals for significance tests for each neuron individually. A neuron was considered significantly locomotion responsive if its 95% confidence interval was significantly different from an LMI of 0 and its value exceeded an LMI of 0.2 (at least 50% change in $\Delta F/F_0$ between locomotion and stationary).

To evaluate the variability of locomotion responses in a given context (dark or visual stimulation) for each neuron, we divided the data in two halves: we calculated separate LMI values for all odd and for all even locomotion periods (Figure 3-figure supplement 1). Neurons with the highest variability of locomotion responses were identified based on the

difference between odd and even LMI values for each neuronal population. The 5% most variable neurons (i.e. neurons that fall outside the red dashed lines Figure 3-figure supplement 1 for either dark or visual stimulation) were excluded from being defined as context-dependent.

Statistics

Error bars in all graphs indicate standard error of the mean (s.e.m.) and statistics were performed with two-tailed tests. Unless otherwise stated, for statistical tests comparing the average $\Delta F/F_0$ of neurons between two contexts or behavioral states (in darkness versus during visual stimulation, or stationary versus locomotion periods) we used Wilcoxon signed-rank tests. For statistical tests comparing the distribution of LMIs and cross-correlations between visual stimulation contexts we used the Kruskal–Wallis test (one-way ANOVA on ranks). For statistical tests comparing $\Delta F/F_0$ values across different layers, Mann-Whitney U tests were used.

For statistical tests we used the number of animals as our sample size because neuronal responses from the same mouse may be correlated and not represent independent samples. Therefore, comparing measures across neurons, rather than across animals, would incorrectly inflate the degrees of freedom with the risk of false positive results for detecting significant differences (Galbraith et al., 2010). This is especially relevant for 2-photon imaging studies where data from a large number of neurons are collected from a small number of animals.

Author contributions

J.P. and N.R. designed the experiments. J.P., E.D., S.C. and N.R. performed the experiments.
J.P., S.L. and C.C. analysed the data. S.L. and S.K. developed the NMF-based neuropil
correction method. J.P. and N.R. wrote the manuscript with input from all authors.

Acknowledgments

We thank Ian Duguid and his research group for advice and support on recordings in awake
mice. We thank Matt Nolan and Ian Duguid for comments on earlier versions of the
manuscript. We thank the GENIE Program and the Janelia Research Campus, specifically V.
Jayaraman, R. Kerr, D. Kim, L. Looger, and K. Svoboda, for making GCaMP6 available.

Competing interests

The authors declare having no competing interest.

References

- Alitto HJ and Dan Y. 2013. Cell-type-specific modulation of neocortical activity by basal
forebrain input. *Front Syst Neurosci* **6**: 79.DOI: 10.3389/fnsys.2012.00079
- Arroyo S, Bennett C, Aziz D, Brown SP and Hestrin S. 2012. Prolonged disynaptic inhibition in
the cortex mediated by slow, non-alpha7 nicotinic excitation of a specific subset of
cortical interneurons. *J Neurosci* **32**: 3859-3864.DOI: 10.1523/JNEUROSCI.0115-
12.2012
- Arroyo S, Bennett C and Hestrin S. 2014. Nicotinic modulation of cortical circuits. *Front
Neural Circuits* **8**: 30.DOI: 10.3389/fncir.2014.00030
- Bennett C, Arroyo S and Hestrin S. 2013. Subthreshold mechanisms underlying state-
dependent modulation of visual responses. *Neuron* **80**: 350-357.DOI:
10.1016/j.neuron.2013.08.007
- Bennett C, Arroyo S and Hestrin S. 2014. Controlling brain states. *Neuron* **83**: 260-261.DOI:
10.1016/j.neuron.2014.07.007
- Brainard DH. 1997. The Psychophysics Toolbox. *Spat Vis* **10**: 433-436
- Chen, Wardill TJ, Sun Y, Pulver SR, Renninger SL, Baohan A, Schreiter ER, Kerr RA, Orger MB,
Jayaraman V, Looger LL, Svoboda K and Kim DS. 2013. Ultrasensitive fluorescent
proteins for imaging neuronal activity. *Nature* **499**: 295-300.DOI:
10.1038/nature12354

605 Chen N, Sugihara H and Sur M. 2015. An acetylcholine-activated microcircuit drives
606 temporal dynamics of cortical activity. *Nat Neurosci* **18**: 892-902.DOI:
607 10.1038/nn.4002

608 Dombeck DA, Khabbazi AN, Collman F, Adelman TL and Tank DW. 2007. Imaging large-scale
609 neural activity with cellular resolution in awake, mobile mice. *Neuron* **56**: 43-57.DOI:
610 10.1016/j.neuron.2007.08.003

611 Erisken S, Vaiceliunaite A, Jurjut O, Fiorini M, Katzner S and Busse L. 2014. Effects of
612 locomotion extend throughout the mouse early visual system. *Curr Biol* **24**: 2899-
613 2907.DOI: 10.1016/j.cub.2014.10.045

614 Fanselow EE, Richardson KA and Connors BW. 2008. Selective, state-dependent activation of
615 somatostatin-expressing inhibitory interneurons in mouse neocortex. *J Neurophysiol*
616 **100**: 2640-2652.DOI: 10.1152/jn.90691.2008

617 Fu Y, Tucciarone JM, Espinosa JS, Sheng N, Darcy DP, Nicoll RA, Huang ZJ and Stryker MP.
618 2014. A cortical circuit for gain control by behavioral state. *Cell* **156**: 1139-1152.DOI:
619 10.1016/j.cell.2014.01.050

620 Fucile S. 2004. Ca²⁺ permeability of nicotinic acetylcholine receptors. *Cell Calcium* **35**: 1-8

621 Galbraith S, Daniel JA and Vissel B. 2010. A study of clustered data and approaches to its
622 analysis. *J Neurosci* **30**: 10601-10608.DOI: 10.1523/JNEUROSCI.0362-10.2010

623 Grienberger C, Rochefort NL, Adelsberger H, Henning HA, Hill DN, Reichwald J, Staufenbiel
624 M and Konnerth A. 2012. Staged decline of neuronal function in vivo in an animal
625 model of Alzheimer's disease. *Nat Commun* **3**: 774.DOI: 10.1038/ncomms1783

626 Iriki A, Tanaka M and Iwamura Y. 1996. Attention-induced neuronal activity in the monkey
627 somatosensory cortex revealed by pupillometrics. *Neurosci Res* **25**: 173-181

628 Jackson J, Ayzenshtat I, Karnani MM and Yuste R. 2016. VIP+ interneurons control
629 neocortical activity across brain states. *J Neurophysiol* **115**: 3008-3017.DOI:
630 10.1152/jn.01124.2015

631 Jiang X, Shen S, Cadwell CR, Berens P, Sinz F, Ecker AS, Patel S and Tolias AS. 2015. Principles
632 of connectivity among morphologically defined cell types in adult neocortex. *Science*
633 **350**: aac9462.DOI: 10.1126/science.aac9462

634 Kaifosh P, Zaremba JD, Danielson NB and Losonczy A. 2014. SIMA: Python software for
635 analysis of dynamic fluorescence imaging data. *Front Neuroinform* **8**: 80.DOI:
636 10.3389/fninf.2014.00080

637 Kawaguchi Y. 1997. Selective cholinergic modulation of cortical GABAergic cell subtypes. *J*
638 *Neurophysiol* **78**: 1743-1747

639 Kawaguchi Y and Shindou T. 1998. Noradrenergic excitation and inhibition of GABAergic cell
640 types in rat frontal cortex. *J Neurosci* **18**: 6963-6976

641 Keller GB, Bonhoeffer T and Hubener M. 2012. Sensorimotor mismatch signals in primary
642 visual cortex of the behaving mouse. *Neuron* **74**: 809-815.DOI:
643 10.1016/j.neuron.2012.03.040

644 Kim H and Park H. 2007. Sparse non-negative matrix factorizations via alternating non-
645 negativity-constrained least squares for microarray data analysis. *Bioinformatics* **23**:
646 1495-1502.DOI: 10.1093/bioinformatics/btm134

647 Kirkwood A, Rozas C, Kirkwood J, Perez F and Bear MF. 1999. Modulation of long-term
648 synaptic depression in visual cortex by acetylcholine and norepinephrine. *J Neurosci*
649 **19**: 1599-1609

- Langville AN, Meyer CD, Albright R, Cox J and Duling D. 2014. Algorithms, initializations, and convergence for the nonnegative matrix factorization. *SAS Technical Report ArXiv:1407.7299*
- Lee AM, Hoy JL, Bonci A, Wilbrecht L, Stryker MP and Niell CM. 2014. Identification of a brainstem circuit regulating visual cortical state in parallel with locomotion. *Neuron* **83**: 455-466.DOI: 10.1016/j.neuron.2014.06.031
- McCormick DA, Wang Z and Huguenard J. 1993. Neurotransmitter control of neocortical neuronal activity and excitability. *Cereb Cortex* **3**: 387-398
- McGinley MJ, Vinck M, Reimer J, Batista-Brito R, Zagha E, Cadwell CR, Tolias AS, Cardin JA and McCormick DA. 2015. Waking State: Rapid Variations Modulate Neural and Behavioral Responses. *Neuron* **87**: 1143-1161.DOI: 10.1016/j.neuron.2015.09.012
- Niell CM. 2015. Cell types, circuits, and receptive fields in the mouse visual cortex. *Annu Rev Neurosci* **38**: 413-431.DOI: 10.1146/annurev-neuro-071714-033807
- Niell CM and Stryker MP. 2010. Modulation of visual responses by behavioral state in mouse visual cortex. *Neuron* **65**: 472-479.DOI: 10.1016/j.neuron.2010.01.033
- Petersen CC and Crochet S. 2013. Synaptic computation and sensory processing in neocortical layer 2/3. *Neuron* **78**: 28-48.DOI: 10.1016/j.neuron.2013.03.020
- Pfeffer CK, Xue M, He M, Huang ZJ and Scanziani M. 2013. Inhibition of inhibition in visual cortex: the logic of connections between molecularly distinct interneurons. *Nat Neurosci* **16**: 1068-1076.DOI: 10.1038/nn.3446
- Pi HJ, Hangya B, Kvitsiani D, Sanders JI, Huang ZJ and Kepecs A. 2013. Cortical interneurons that specialize in disinhibitory control. *Nature* **503**: 521-524.DOI: 10.1038/nature12676
- Pinto L, Goard MJ, Estandian D, Xu M, Kwan AC, Lee SH, Harrison TC, Feng G and Dan Y. 2013. Fast modulation of visual perception by basal forebrain cholinergic neurons. *Nat Neurosci* **16**: 1857-1863.DOI: 10.1038/nn.3552
- Polack PO, Friedman J and Golshani P. 2013. Cellular mechanisms of brain state-dependent gain modulation in visual cortex. *Nat Neurosci* **16**: 1331-1339.DOI: 10.1038/nn.3464
- Reimer J, Froudarakis E, Cadwell CR, Yatsenko D, Denfield GH and Tolias AS. 2014. Pupil fluctuations track fast switching of cortical states during quiet wakefulness. *Neuron* **84**: 355-362.DOI: 10.1016/j.neuron.2014.09.033
- Roth MM, Dahmen JC, Muir DR, Imhof F, Martini FJ and Hofer SB. 2016. Thalamic nuclei convey diverse contextual information to layer 1 of visual cortex. *Nat Neurosci* **19**: 299-307.DOI: 10.1038/nn.4197
- Saleem AB, Ayaz A, Jeffery KJ, Harris KD and Carandini M. 2013. Integration of visual motion and locomotion in mouse visual cortex. *Nat Neurosci* **16**: 1864-1869.DOI: 10.1038/nn.3567
- Shen JX and Yakel JL. 2009. Nicotinic acetylcholine receptor-mediated calcium signaling in the nervous system. *Acta Pharmacol Sin* **30**: 673-680.DOI: 10.1038/aps.2009.64
- Urban-Ciecko J and Barth AL. 2016. Somatostatin-expressing neurons in cortical networks. *Nat Rev Neurosci*.DOI: 10.1038/nrn.2016.53
- Xiang Z, Huguenard JR and Prince DA. 1998. Cholinergic switching within neocortical inhibitory networks. *Science* **281**: 985-988
- Xu H, Jeong HY, Tremblay R and Rudy B. 2013. Neocortical somatostatin-expressing GABAergic interneurons disinhibit the thalamorecipient layer 4. *Neuron* **77**: 155-167.DOI: 10.1016/j.neuron.2012.11.004

Žitnik M and Zupan B. 2012. NIMFA: a python library for nonnegative matrix factorization. *J. Mach. Learn. Res.* **13**: 849-853

Figure Legends

Figure 1. Imaging locomotion responses of excitatory and inhibitory neurons in mouse V1.

(A) Schematic of the connectivity between pyramidal neurons (Pyr) and subtypes of inhibitory neurons, vasoactive intestinal peptide (VIP), somatostatin (SST) and parvalbumin (PV) expressing neurons, established from in vitro studies in V1 (Pfeffer et al., 2013; Jiang et al., 2015). (B) Proposed disinhibition model: locomotion activates VIP neurons through cholinergic (ACh) inputs, SST neurons are inhibited, which leads to a disinhibition of Pyr neurons and an increase in the gain of visual responses during locomotion (Fu et al., 2014). (C) Experimental set-up for two-photon calcium imaging in V1 of awake-behaving mice. Mice are head-fixed and can run freely on a cylindrical treadmill either during the presentation of a visual stimulus (oriented gratings) or in darkness. (D) Confocal images of 50 μm thick coronal sections showing cell type specific GCaMP6f expression in VIP, SST and PV-positive inhibitory neurons as well as in CaMKII-positive excitatory populations. Boundaries between cortical layers are indicated. (E) Left panel, in vivo two-photon images of VIP, SST and PV neurons labelled with GCaMP6f; cortical depth of imaging is indicated. Right panel, example calcium transients ($\Delta F/F_0$, coloured traces) of single VIP, SST and PV neurons, imaged in darkness and during visual stimulation with oriented gratings (grey bar above trace), and aligned with the corresponding running speed (cm/s, black traces). Scale bars on images, 50 μm .

Figure 2. Locomotion differentially modulates excitatory and inhibitory neuronal responses in darkness and during visual stimulation in V1 layer 2/3. (A-B) Scatter plots of the mean amplitude of fluorescence changes ($\Delta F/F_0$) of each neuron for locomotion periods versus stationary periods, in darkness (A) and during visual stimulation (oriented gratings) (B); (i) excitatory cells (Exc), $n=1124$; (ii) VIP, $n=210$; (iii) SST, $n=79$; (iv) PV, $n=199$ neurons. (C) Histograms of the distribution of locomotion modulation indices ($\text{LMI} = (R_L - R_S)/(R_L + R_S)$, where R_L and R_S are the mean $\Delta F/F_0$ during locomotion and stationary periods, respectively), for each cell type, in darkness (Dark, black) and during visual stimulation (Stim, coloured). An LMI equal to 0 indicates no difference between locomotion and stationary periods, while an LMI equal to 0.5 indicates that the average amplitude of calcium transients was three times higher during locomotion than during stationary periods. (D) Mean of the median LMI per animal and s.e.m. ** $p < 0.01$, n.s., not significant ($p > 0.05$); $n = 12$ (i), 12(ii), 11(iii), 13(iv) mice; Kruskal–Wallis test. (E) Schematic representation of the results. Size and direction of arrows indicate the average response per cell type during locomotion (increasing or decreasing activity). In darkness, SST and excitatory neurons were largely non-responsive to locomotion while VIP and PV neurons

were strongly activated by locomotion. However, during visual stimulation, locomotion increases the responses of excitatory neurons as well as of the three classes of inhibitory neurons (VIP, SST and PV).

Figure 2-figure supplement 1. Modulation of excitatory and inhibitory neurons responses by locomotion during the presentation of patterned (oriented gratings) and non-patterned (grey screen) visual stimuli. (A) Scatter plots of the mean amplitude of fluorescence changes (mean $\Delta F/F_0$) of each neuron for locomotion periods versus stationary periods, during grey screen presentation; (i) excitatory cells (Exc), $n=1124$; (ii) VIP, $n=210$; (iii) SST, $n=79$; (iv) PV, $n=199$ neurons. (B) Mean $\Delta F/F_0$ per animal and s.e.m. for stationary (open bars) and locomotion (solid bars) periods in darkness (Dark), during grey screen presentation (Grey), and during the presentation of oriented gratings (Stim); statistics based on Wilcoxon signed rank test. (C) Mean of the median LMI per animal and s.e.m.; statistics based on Kruskal–Wallis test. For (B-C), $n= 12$ (i), 12 (ii), 11 (iii), 13 (iv) mice; * $p<0.05$, ** $P<0.01$ and *** $P<0.001$, n.s., not significant ($p>0.05$).

Figure 2-figure supplement 2. Visual responsiveness of excitatory and inhibitory neurons during stationary and locomotion periods. (A-B) Scatter plots of the mean amplitude of fluorescence changes ($\Delta F/F_0$) of each neuron during visual stimulation (oriented gratings) versus darkness, during stationary (A) and locomotion (B) periods. (C) Mean $\Delta F/F_0$ per animal and s.e.m. in darkness (Dark, black bars) versus during the presentation of visual stimulation (oriented gratings; Stim, coloured bars) during stationary and locomotion periods; statistics based on Wilcoxon signed rank test; $n= 12$ (i), 12 (ii), 11 (iii), 13 (iv) mice; * $p<0.05$, ** $P<0.01$ and *** $P<0.001$, n.s., not significant ($p>0.05$).

Figure 2-figure supplement 3. Cross correlation of fluorescence changes ($\Delta F/F_0$) with running speed. (A) Cross-correlation between $\Delta F/F_0$ and running speed during darkness (left) and visual stimulation (right) for each neuronal subtype. Thin grey lines represent individual neurons and thick lines represent the mean cross-correlation across all neurons within a subtype. (B) Histograms of the zero-time correlation values per neuron in darkness (dark bars) and during visual stimulation (coloured bars). (C) Mean zero-time correlation and s.e.m. for each neuronal subtype across animals, in darkness (left) and during visual stimulation (middle). Right panel shows the difference between darkness and visual stimulation conditions (mean zero-time values, Stim-Dark). Note that SST neurons show significantly higher zero-time correlation values during visual stimulation ($p=0.001$), as do excitatory neurons ($p=0.024$). In contrast, VIP neurons have lower zero-time correlation values during visual stimulation, however this difference is not significant across animals ($p=0.225$). PV neurons show no significant change between darkness and visual stimulation conditions ($p=0.778$).

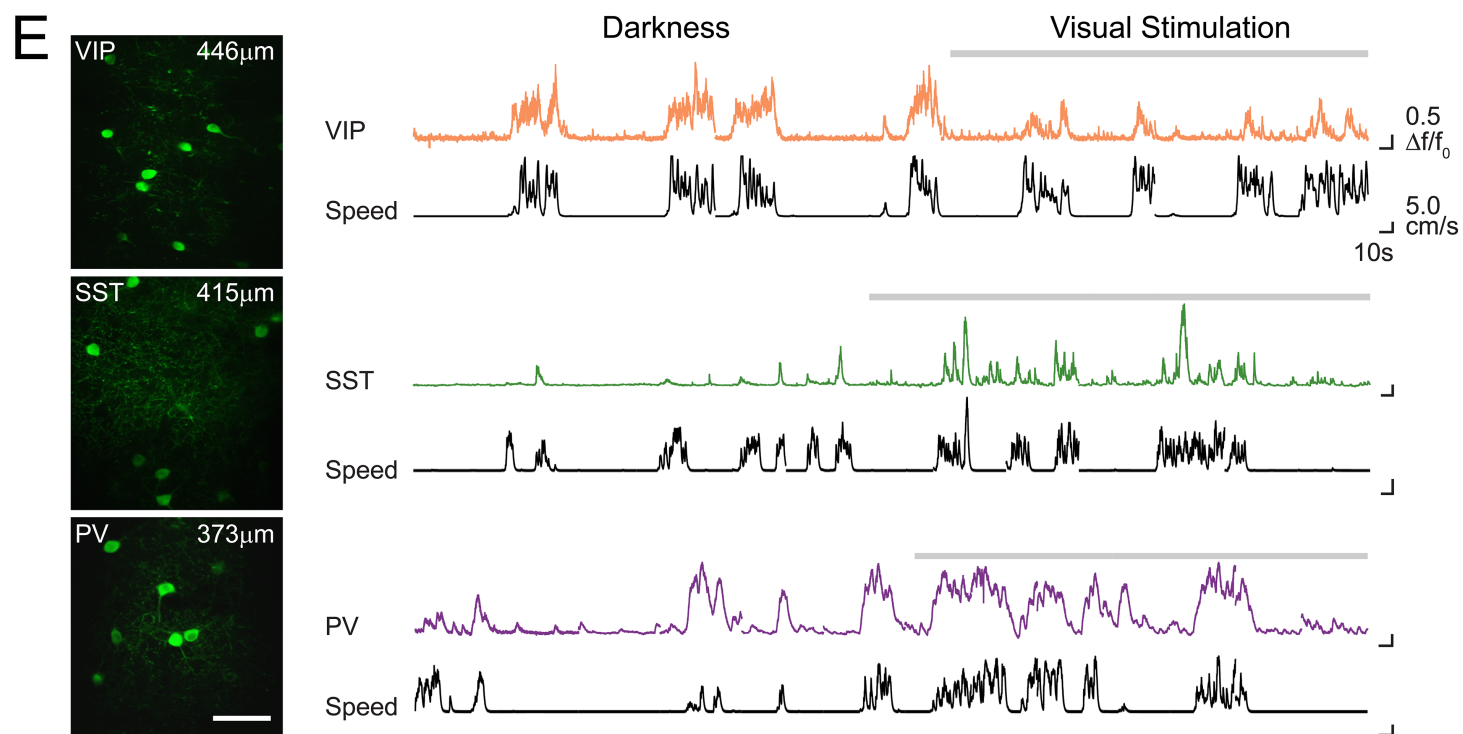
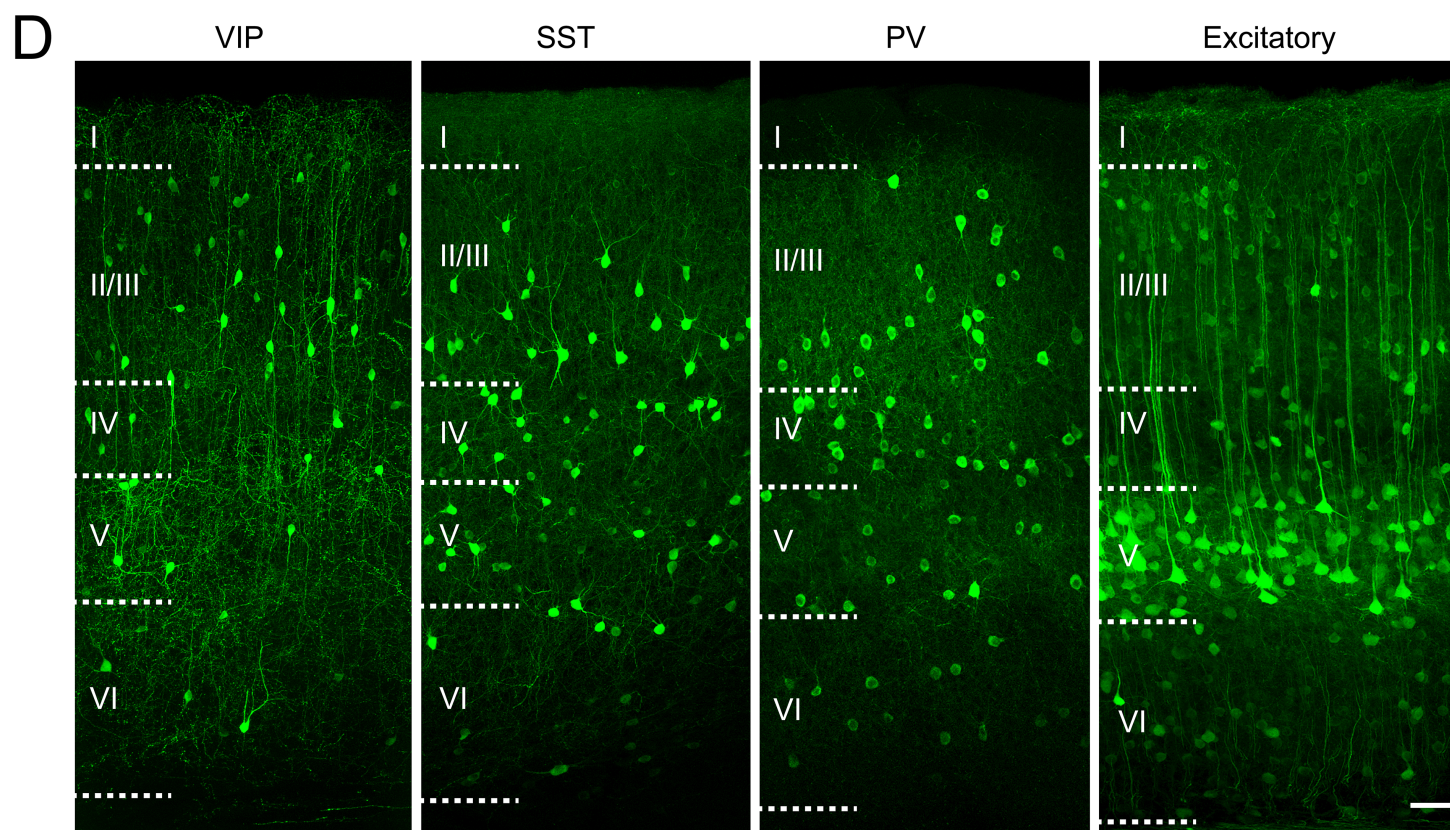
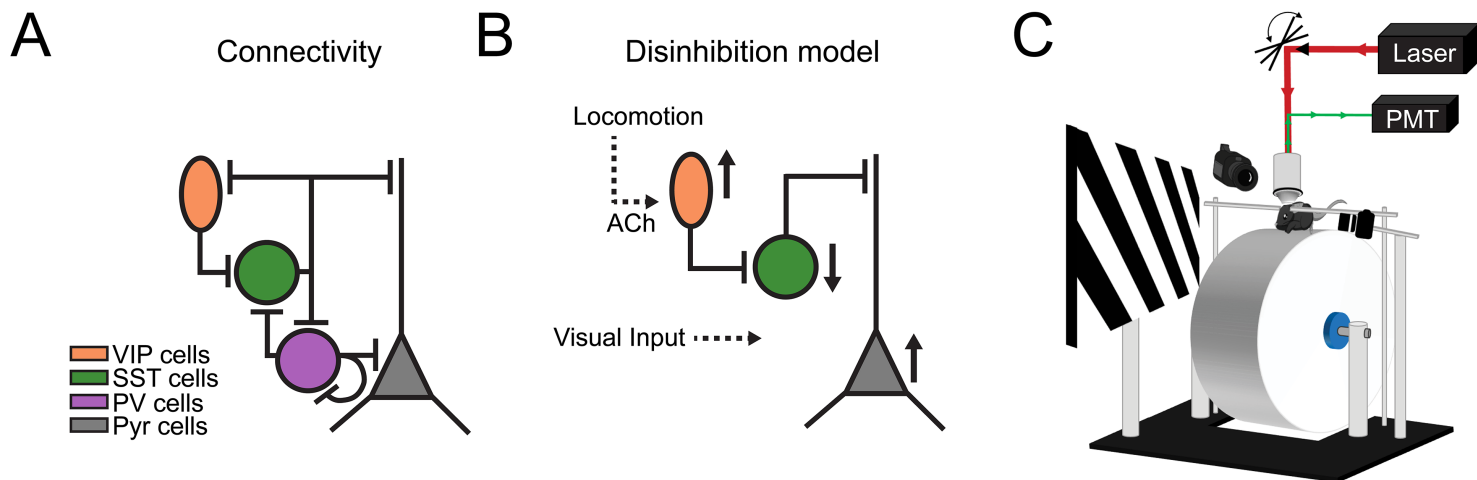
Figure 3. Context-dependent responses to locomotion of individual excitatory and inhibitory neurons in layer 2/3. (A) Left panels, scatter plots of the locomotion modulation index (LMI) of individual neurons in darkness versus during visual stimulation (gratings) with associated Pearson correlation coefficient (R-values). Context-dependent (CD; red) and context-independent (CI; blue) locomotion responsive neurons are highlighted. Context dependency was defined for each neuron by its distance from the identity line and the variability of its locomotion responses (see Materials and methods and Figure3-figure supplement 1). Neurons that were either non-responsive to locomotion or responded unreliably are shown as open circles. Right panels, percentages of context-dependent (CD) and context-independent (CI) neurons for each neuronal subtype. Note the high proportion of CI VIP neurons (66%), the high proportion of CD SST neurons (49%), and the diversity of both PV and excitatory (Exc) neurons. (B) Histograms of the difference between the LMI value in darkness and during visual stimulation ($LMI_{Stim} - LMI_{Dark}$) for each neuronal population. Negative values indicate increased responses to locomotion in darkness compared with visual stimulation, positive numbers indicate increased responses to locomotion during visual stimulation, and numbers close to 0 (within red lines; $-0.2 < LMI_{Stim} - LMI_{Dark} < 0.2$) indicate context-independent responses.

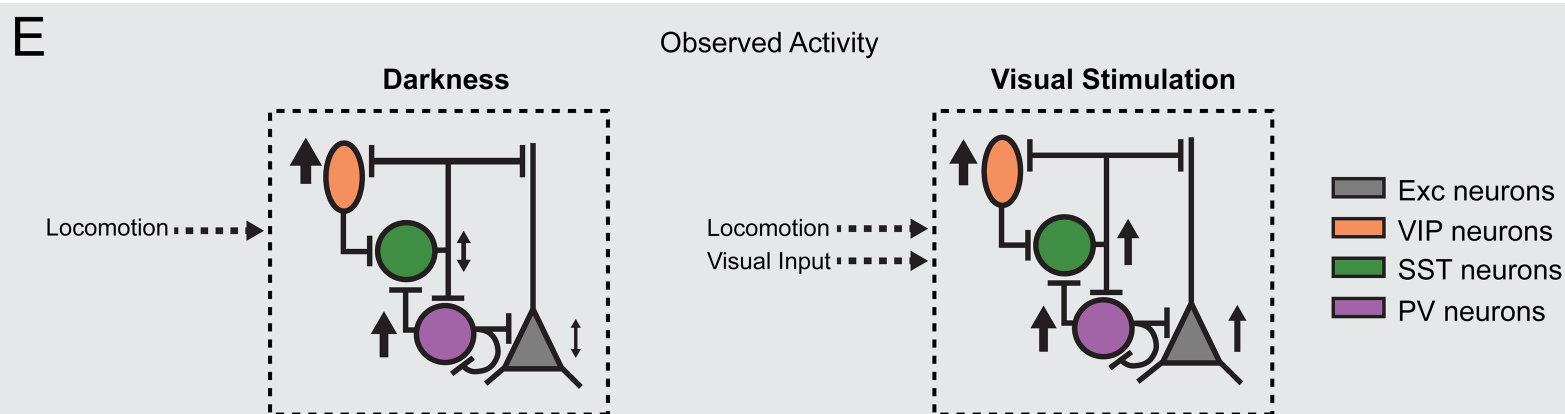
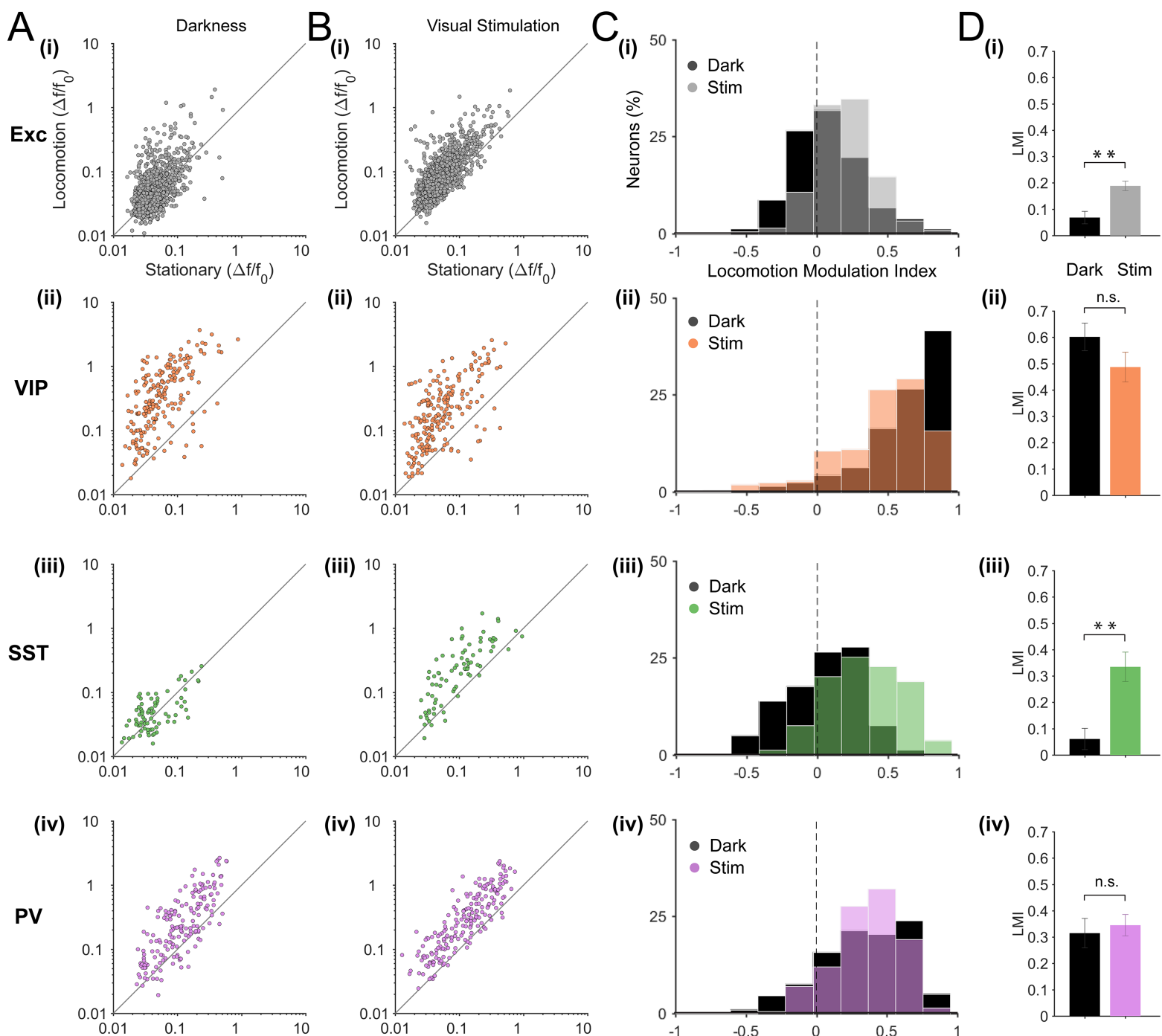
Figure 3-figure supplement 1. Variability of locomotion responses in darkness and during visual stimulation. (A-B) Scatter plots of LMI values calculated for each neuron from their responses during even and odd locomotion and stationary periods, in darkness (A) and during visual stimulation (oriented gratings) (B). Individual periods of locomotion separated by stationary periods (epochs) were divided into odd and even epochs and mean LMIs were calculated for each context (darkness and visual stimulation). Pearson correlation coefficient R-values are shown for each scatter plot. Note the high correlation values for all neuronal populations both in darkness and during visual stimulation ($p < 0.001$). Red lines delineate 5% of the neurons with the highest variability, as measured by the difference in LMI during odd and even epochs. Context-dependent (red) and context-independent (blue) locomotion responsive neurons identified in Figure 3A are highlighted.

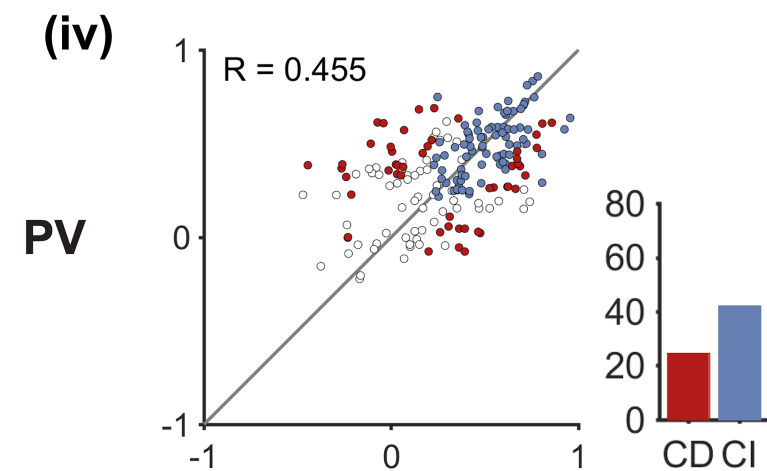
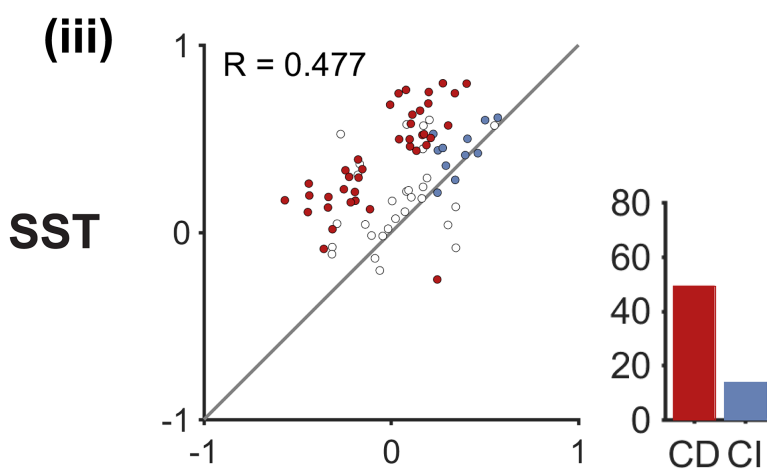
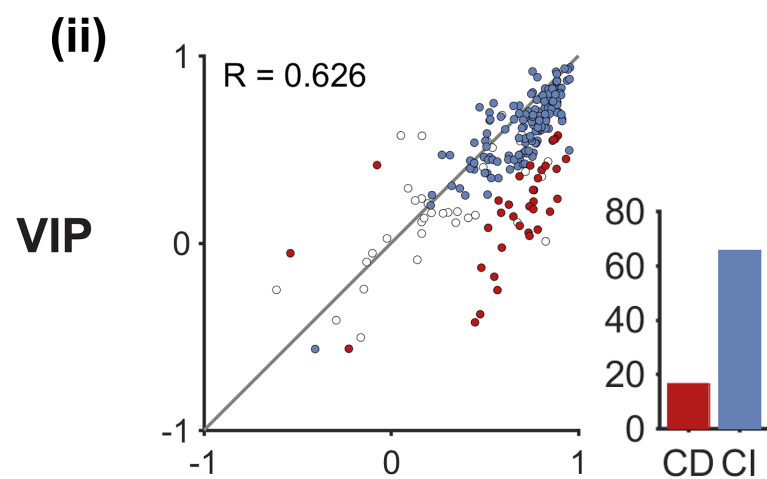
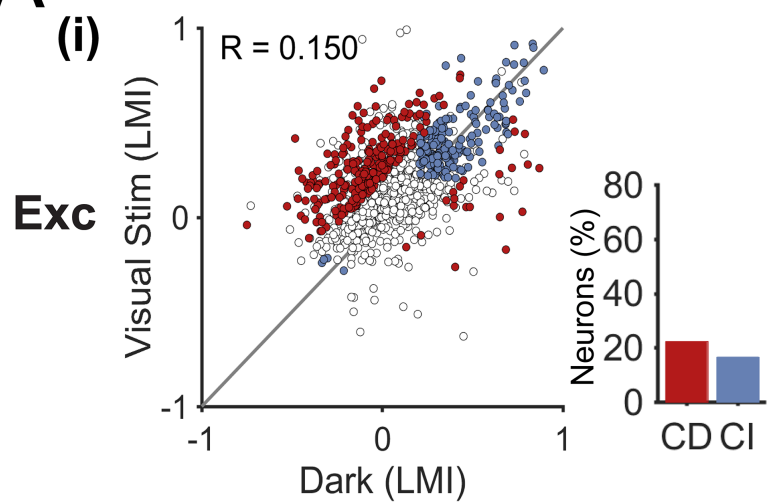
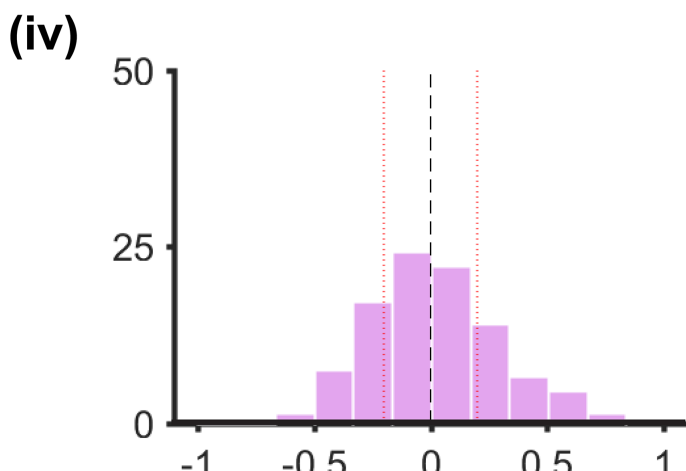
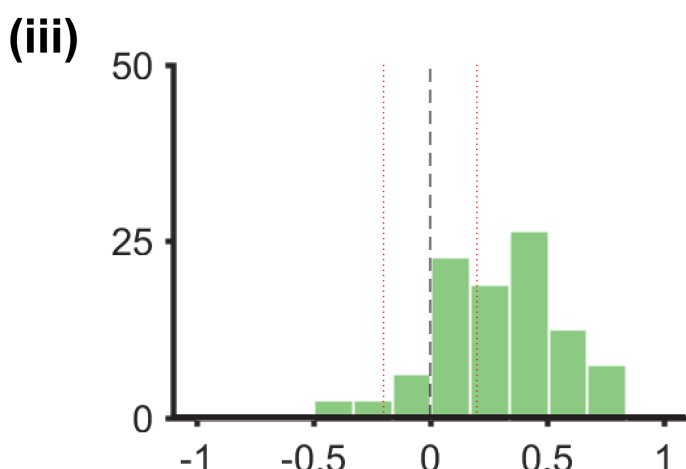
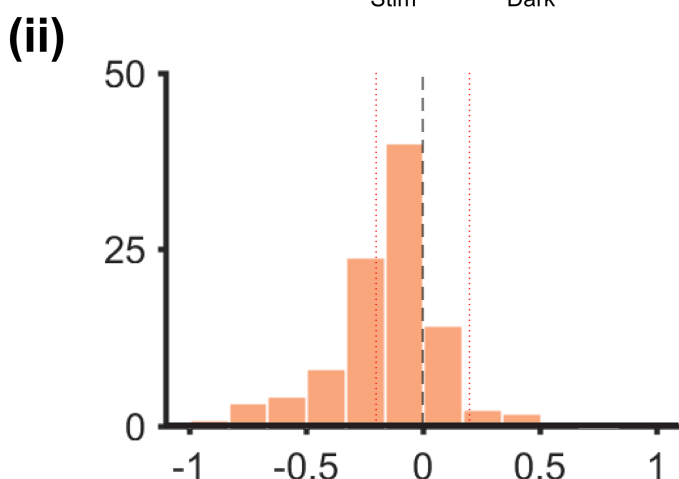
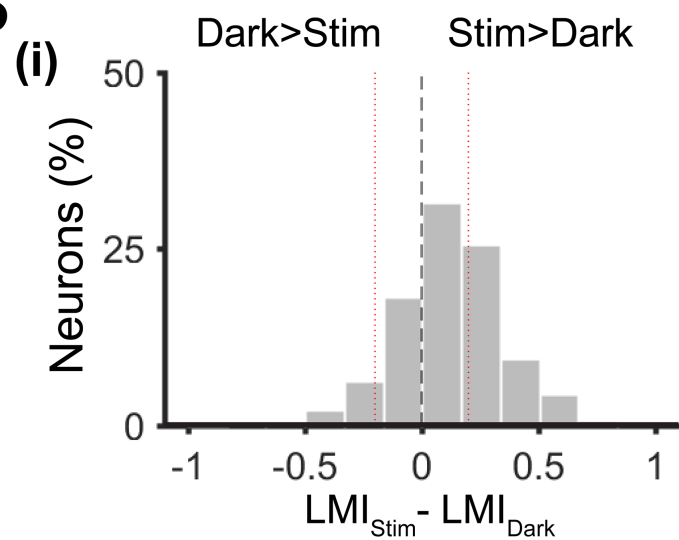
Figure 3-figure supplement 2. Representative examples of calcium transients ($\Delta F/F_0$) of context-independent and context-dependent neurons, in darkness and during visual stimulation with oriented gratings (grey bar above trace). The corresponding running speed is shown below each trace (cm/s, black). Exc, excitatory neuron.

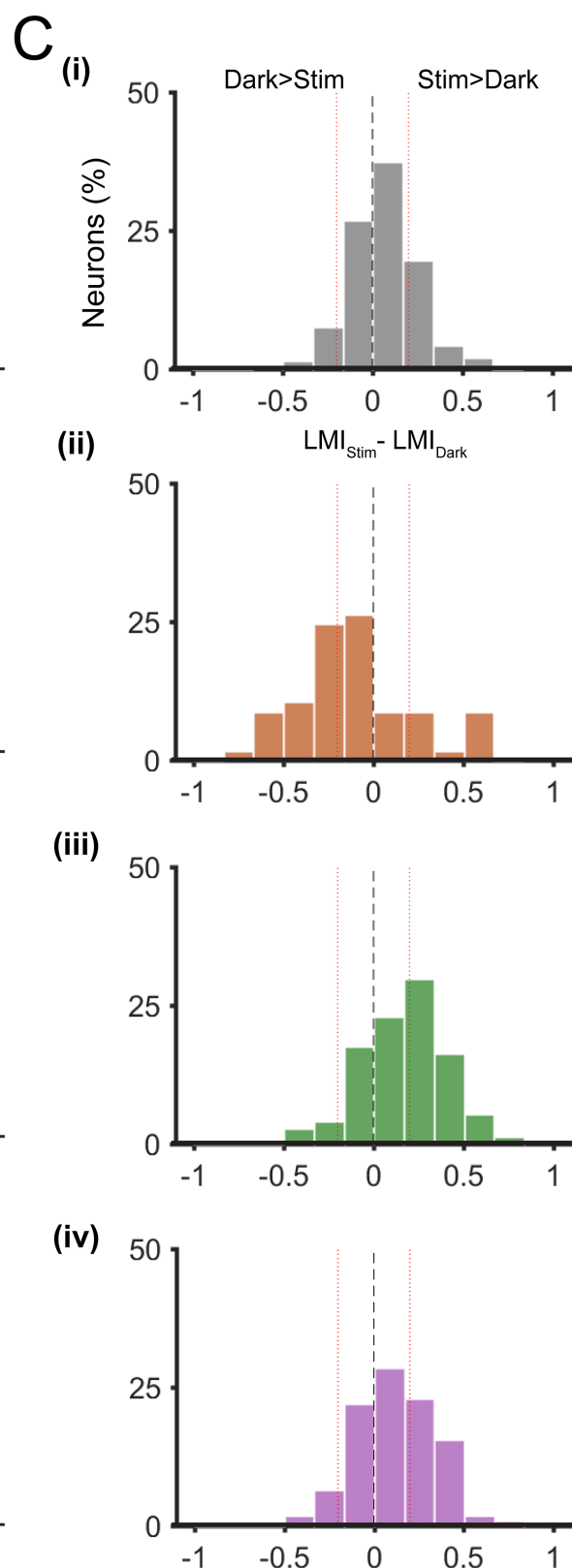
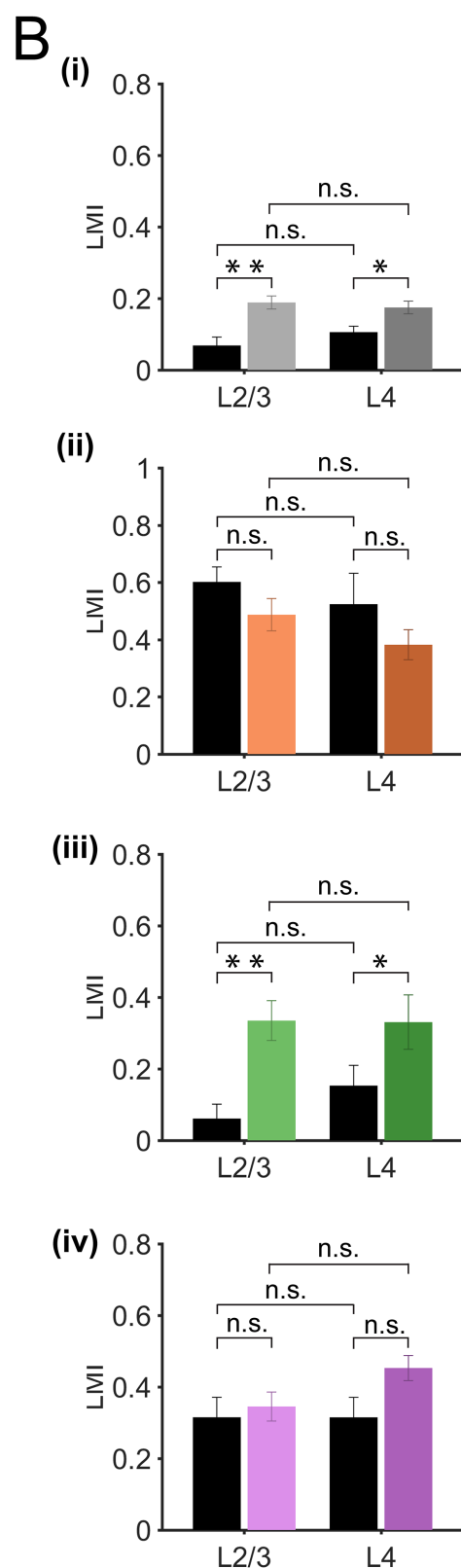
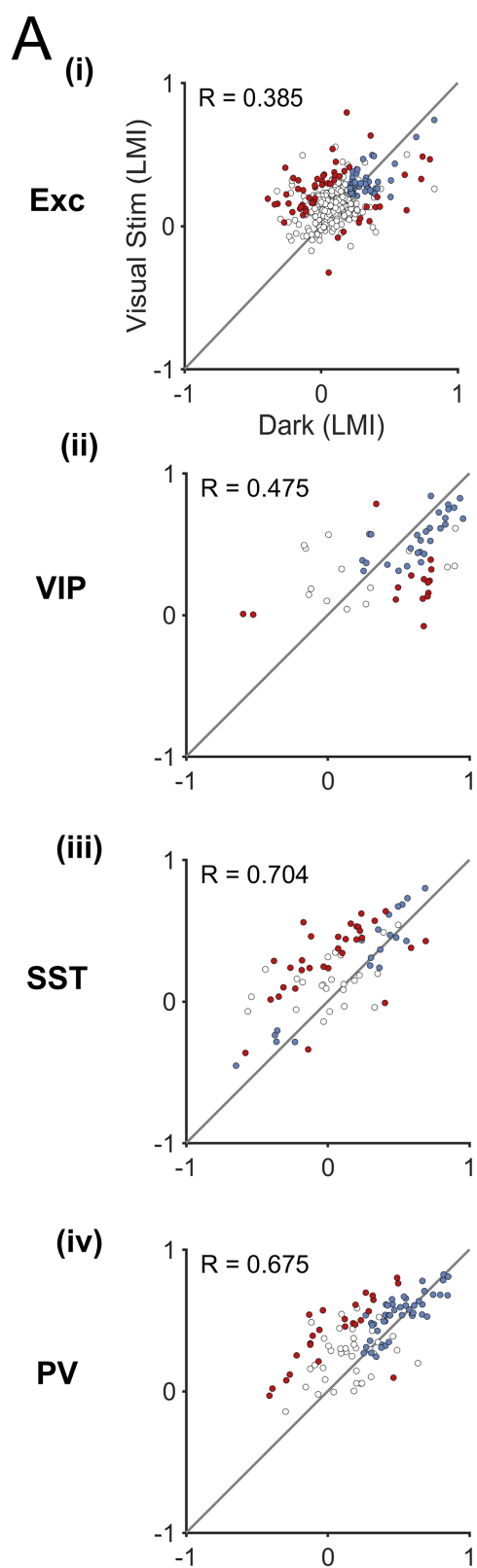
Figure 4. Locomotion responses of individual inhibitory and excitatory neurons in V1 cortical layer 4. (A) Scatter plots of locomotion modulation index (LMI) of individual neurons in darkness versus during visual stimulation (oriented gratings), with associated Pearson correlation coefficient (R-values) for excitatory (Exc; $n = 331$), VIP ($n = 57$), SST ($n = 74$), and PV ($n = 109$) neurons. Context-dependent (red) and context-independent (blue)

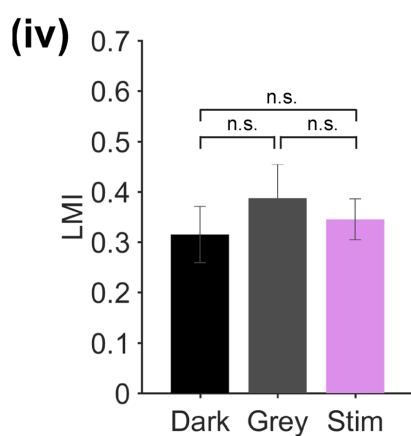
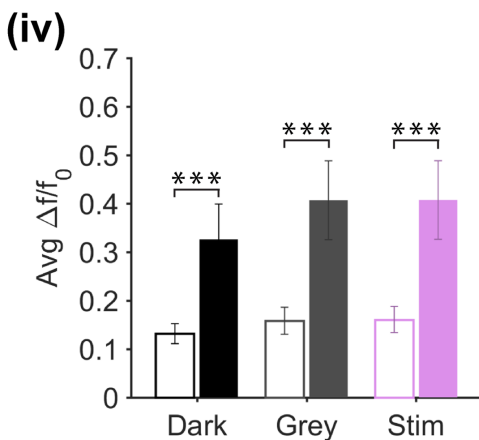
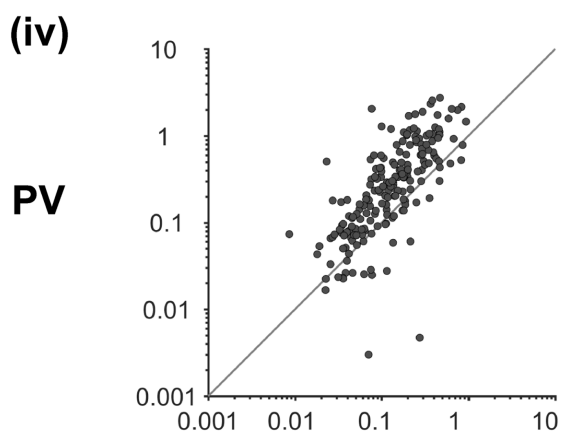
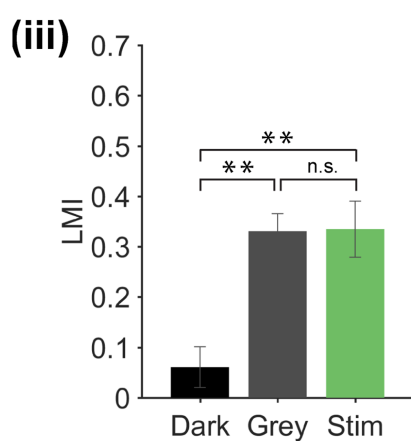
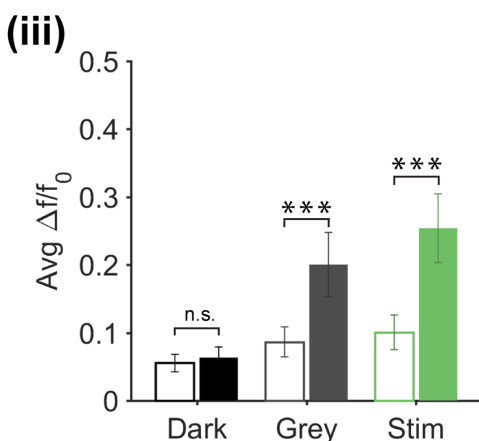
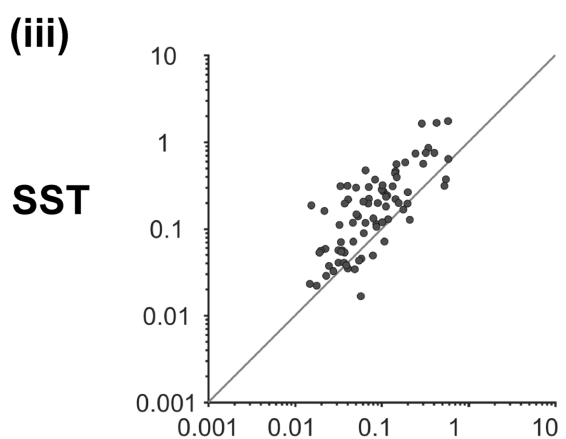
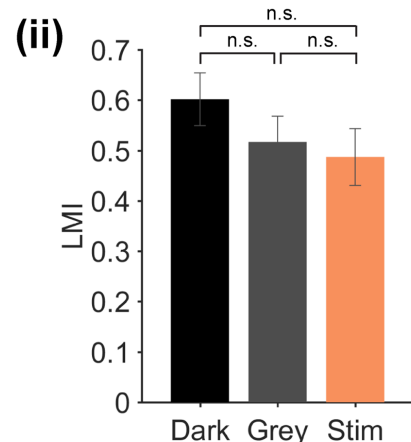
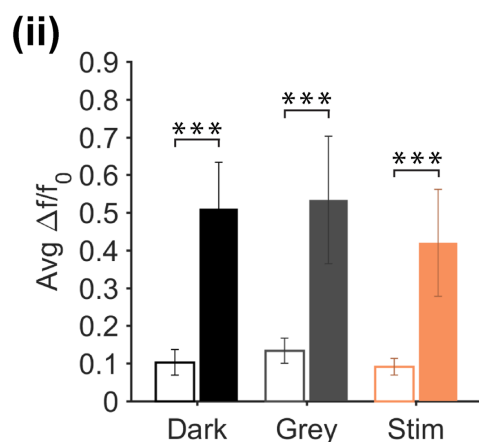
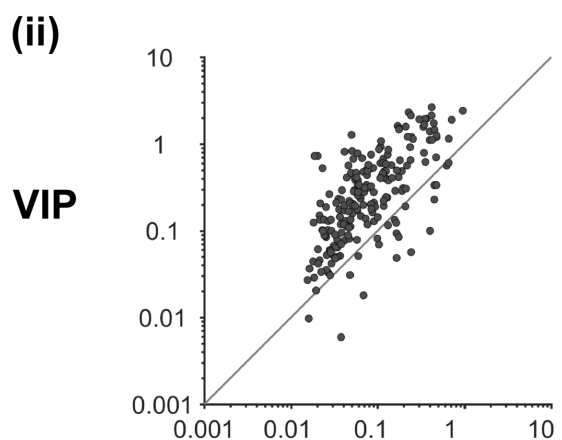
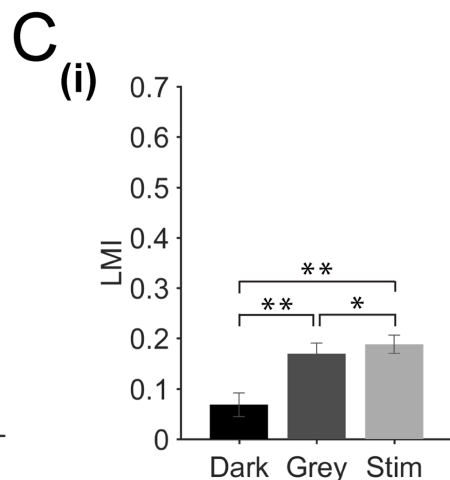
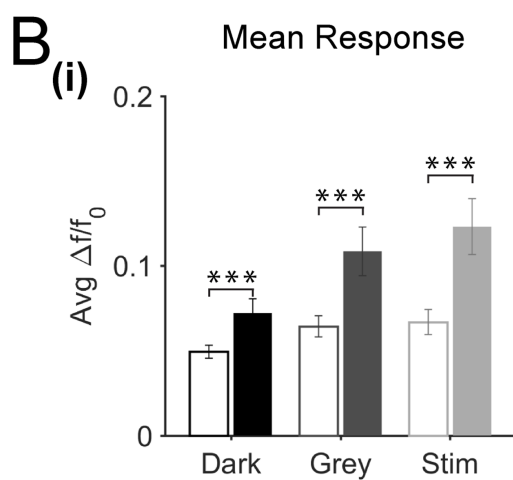
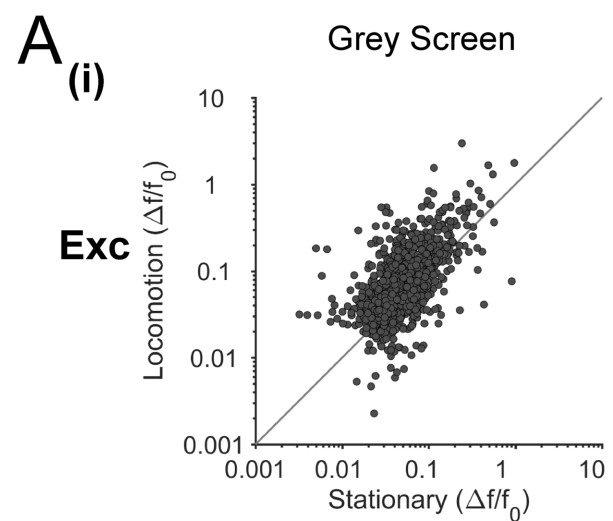
locomotion responsive neurons are highlighted. Context dependency per neuron was defined by its distance from the identity line and its variability to locomotion periods (see Material and methods). Neurons that were either non-responsive to locomotion or responded unreliably are shown as open circles. (B) Mean of the median LMI per animal and s.e.m. for layer 2/3 (L2/3) as well as layer 4 (L4), in darkness (Dark, black bars) and during visual stimulation (Stim, coloured bars) for Exc (L2/3, n=12; L4, n= 6), VIP (L2/3, n= 12; L4, n = 4), SST (L2/3, n= 11; L4, n = 6), and PV (L2/3, n=13; L4, n=6) mice. Within each cell type, there was no significant difference (n.s., $p>0.05$, Mann-Whitney U test) between the median LMI across layers in either context (darkness: Exc, $p=0.151$; VIP, $p=0.521$; SST, $p=0.350$; PV, $p=0.966$; visual stimulation: Exc, $p=0.750$; VIP, $p=0.133$; SST, $p=0.961$; PV, $p=0.058$; (C) Histograms of the difference between the LMI value in darkness and during visual stimulation ($LMI_{Stim}-LMI_{Dark}$) for each cell type. Negative values indicate increased responses to locomotion in the dark compared with visual stimulation, positive numbers indicate increased responses to locomotion during visual stimulation, and numbers close to 0 (within red lines; $-0.2<LMI_{Stim}-LMI_{Dark}<0.2$) indicate context-independent responses.

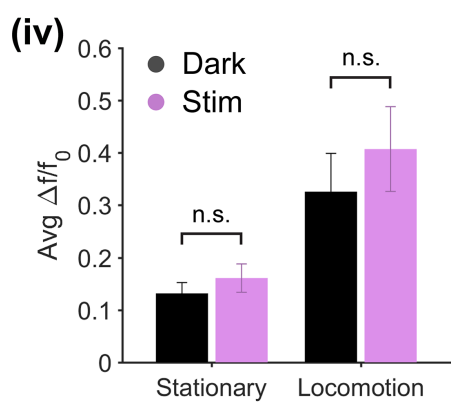
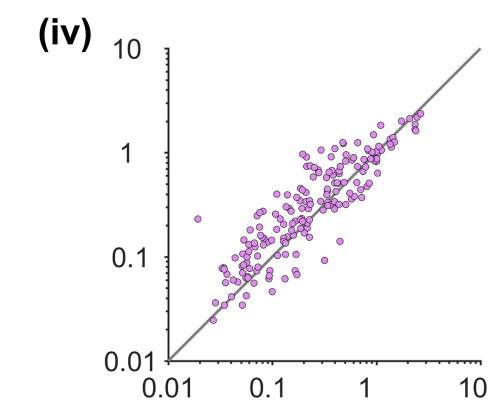
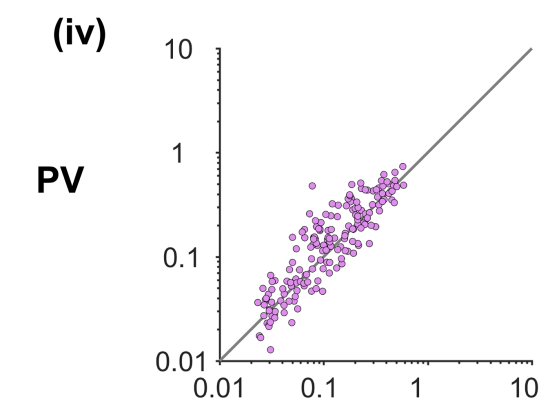
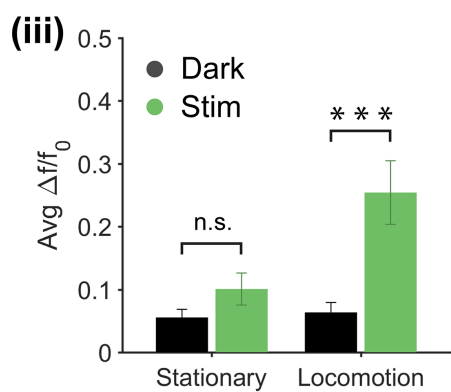
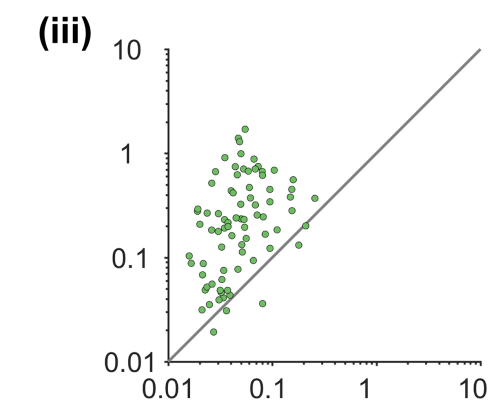
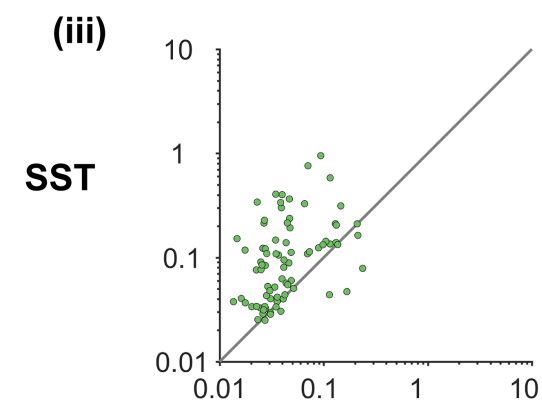
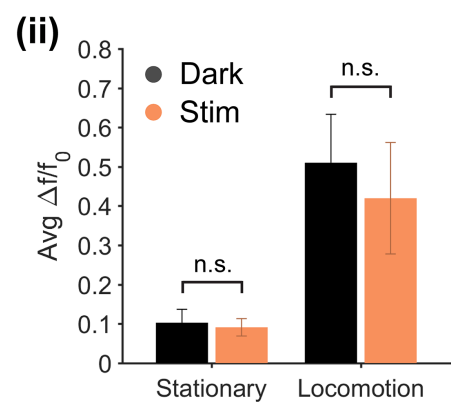
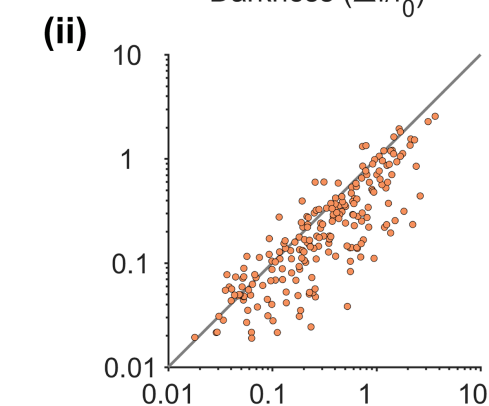
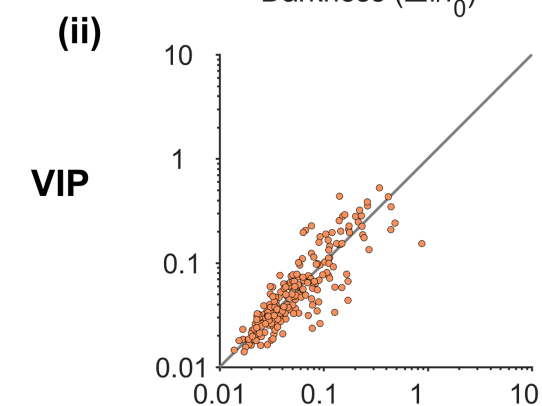
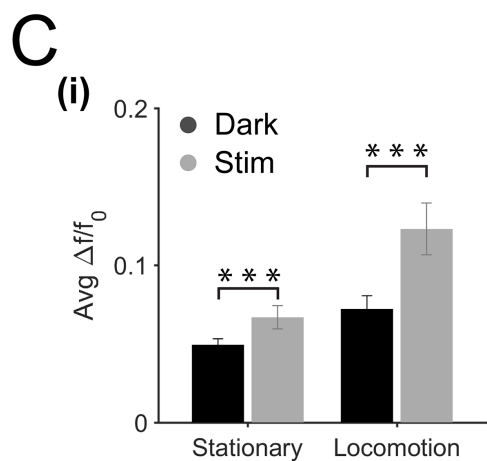
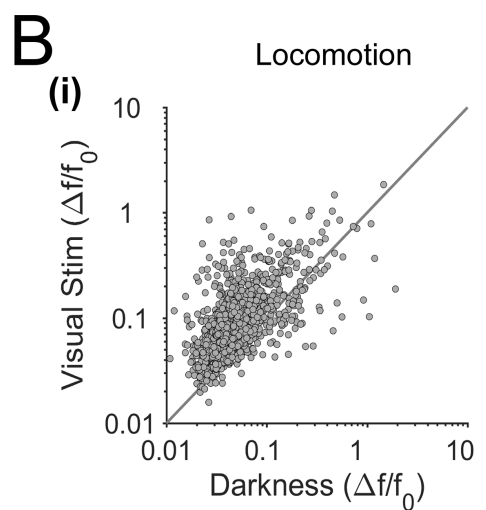
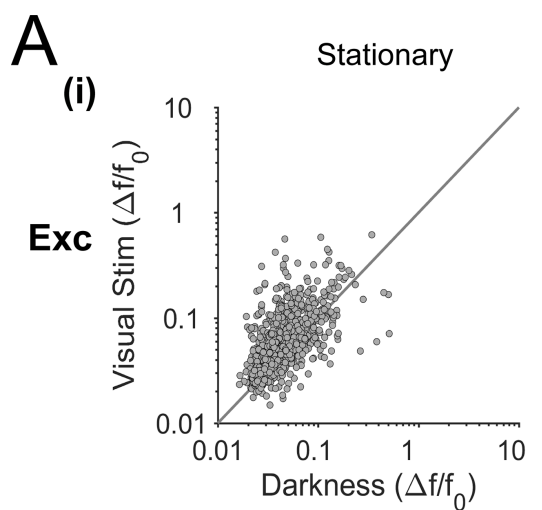


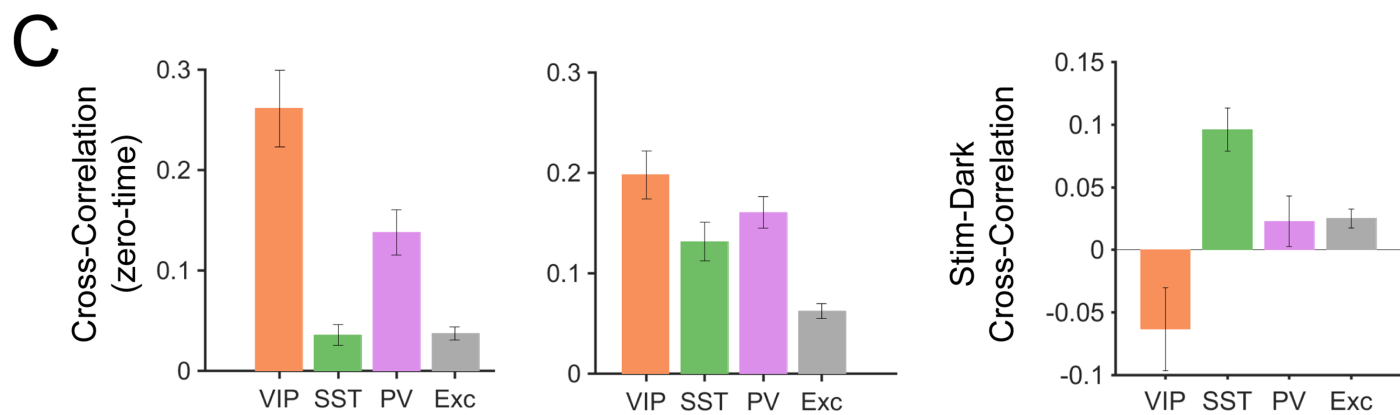
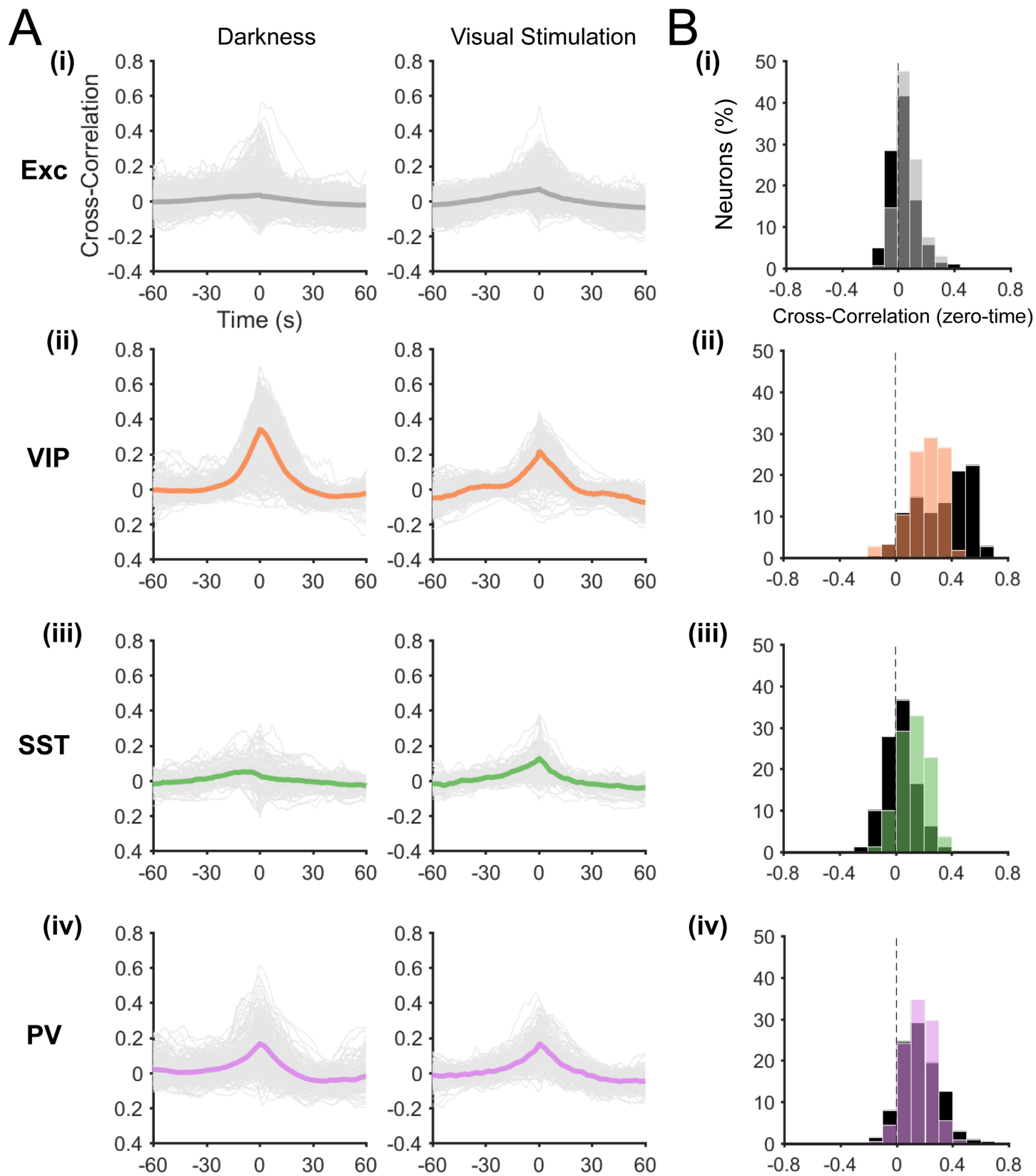


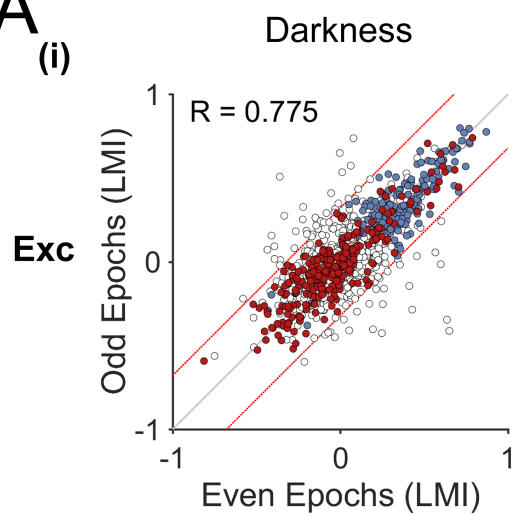
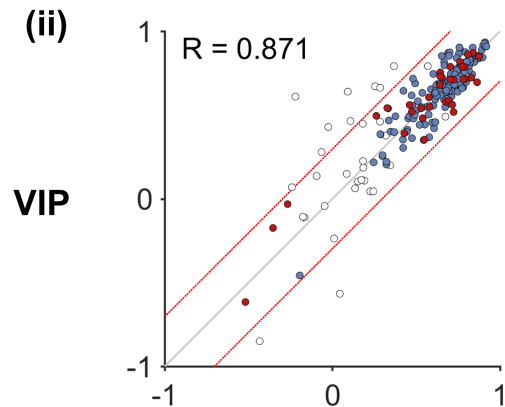
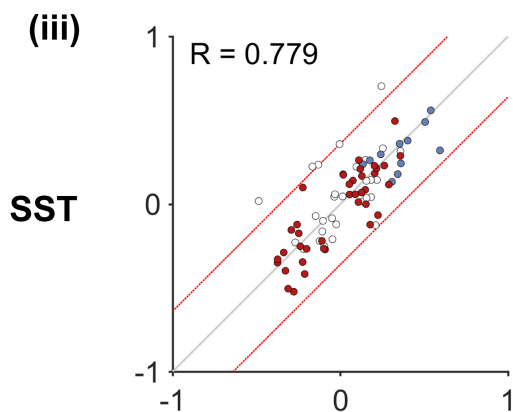
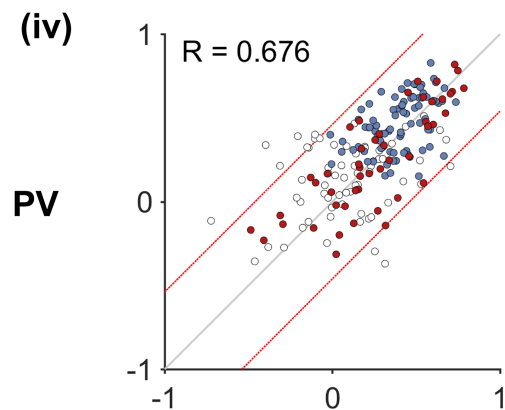
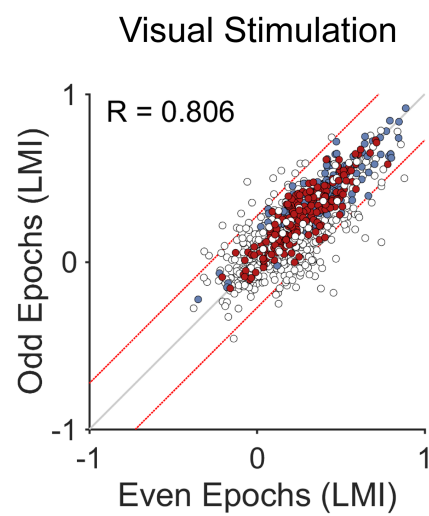
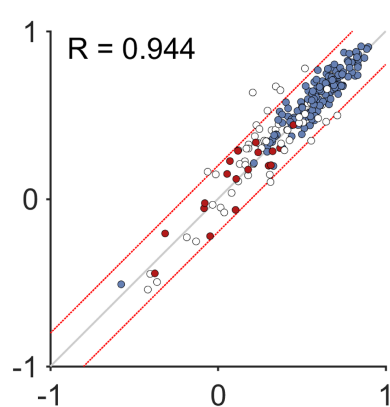
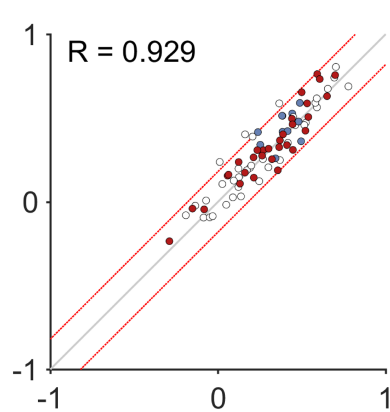
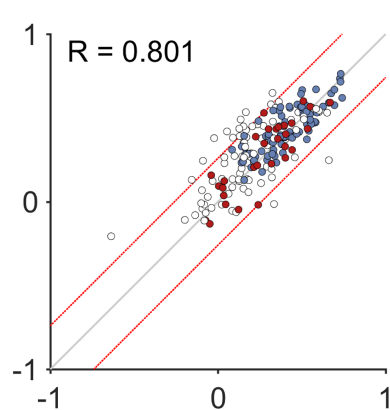
A**B**



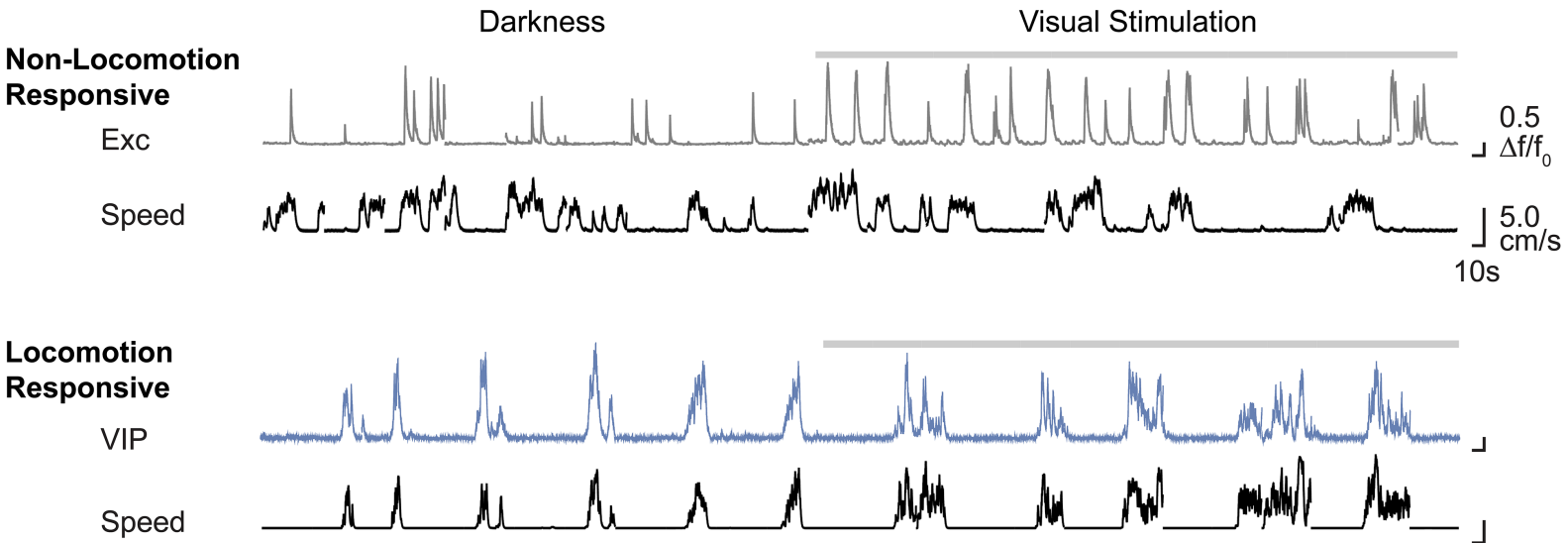






A**(i)****(ii)****(iii)****(iv)****B****(i)****(ii)****(iii)****(iv)**

Context-Independent



Context-dependent

